Physics & Diagnostics of Magnetic Flux Emergence

Mark Cheung[1,2], M. Rempel[3] , G. Chintzoglou[1,4], F. Chen[5] , P. Testa[6],
J. Martínez-Sykora[1,7], B. De Pontieu[1], V. Hansteen[8], and M. Jin[1,9]
1. Lockheed Martin Solar & Astrophysics Laboratory, USA
2. Stanford University, USA
3. National Center for Atmospheric Research, USA
4. University Corporation for Atmospheric Research, USA
5. National Solar Observatory, USA
6. Smithsonian Astrophysical Observatory, USA
7. Bay Area Environmental Research Institute, USA
8. Rosseland Centre for Solar Physics, University of Oslo, Norway
9. SETI Institute, USA

#ESTScienceMeeting
June 11th-15th 2018, Giardini Naxos, Italy

2017-08-18T05:48

A *fluid* view of MHD

Magnetohydrodynamics (MHD) captures the following physical principles:

- Mass conservation, $\frac{D\varrho}{Dt} + \varrho \nabla \cdot \mathbf{v} = 0\,,$

- Momentum conservation,

$$\varrho \frac{D\mathbf{v}}{Dt} = \nabla \cdot \sigma + \varrho \mathbf{g},$$

$$\sigma_{ij} = -p\delta_{ij} + M_{ij},$$
$$M_{ij} = -\frac{B^2}{8\pi}\delta_{ij} + \frac{B_i B_j}{4\pi}.$$

- Energy conservation, $\varrho \frac{Ds}{Dt} = \frac{Q}{T}\,,$

- Faraday's law of induction. (next slide)

Faraday's Induction Equation

Faraday's induction equation is

$$\frac{\partial \mathbf{B}}{\partial t} = -c\nabla \times \mathbf{E}, \tag{8}$$

where $\mathbf{E}$ is the electric field and c is the speed of light. In the regime of ideal MHD where the plasma is a perfect electrical conductor the electric field $\mathbf{E}'$ in the co-moving inertial frame of the plasma vanishes. Assuming the plasma velocity $\mathbf{v}$ has speed $|v| \ll c$, a Lorentz transformation to the 'lab' frame leads to

$$\mathbf{E} = -c^{-1}\mathbf{v} \times \mathbf{B}\,. \tag{9}$$

This yields the familiar Eulerian form of the ideal MHD induction equation

$$\frac{\partial \mathbf{B}}{\partial t} = \nabla \times (\mathbf{v} \times \mathbf{B})\,. \tag{10}$$

In Lagrangian form, this equation becomes

$$\frac{D\mathbf{B}}{Dt} = -\mathbf{B}(\nabla \cdot \mathbf{v}) + (\mathbf{B} \cdot \nabla)\mathbf{v}\,. \tag{11}$$

Fluid expansion / compression

Stretching flow along magnetic field lines intensifies B

Faraday's Induction Equation

Faraday's induction equation is

$$\frac{\partial \mathbf{B}}{\partial t} = -c\nabla \times \mathbf{E}, \tag{8}$$

where $\mathbf{E}$ is the electric field and c is the speed of light. In the regime of ideal MHD where the plasma is a perfect electrical conductor the electric field $\mathbf{E}'$ in the co-moving inertial frame of the plasma vanishes. Assuming the plasma velocity $\mathbf{v}$ has speed $|v| \ll c$, a Lorentz transformation to the 'lab' frame leads to

$$\mathbf{E} = -c^{-1}\mathbf{v} \times \mathbf{B}\,. \tag{9}$$

This yields the familiar Eulerian form of the ideal MHD induction equation

$$\frac{\partial \mathbf{B}}{\partial t} = \nabla \times (\mathbf{v} \times \mathbf{B})\,. \tag{10}$$

In Lagrangian form, this equation becomes

$$\frac{D\mathbf{B}}{Dt} = -\mathbf{B}(\nabla \cdot \mathbf{v}) + (\mathbf{B} \cdot \nabla)\mathbf{v}\,. \tag{11}$$

Fluid expansion / compression

Stretching flow along magnetic field lines intensifies B

Constitutive Relations

Equation of State $p = p(\varrho,\varepsilon)$, $s = s(\varrho,\varepsilon)$, $T = T(\varrho,\varepsilon)$ (only in LTE)

Ohm's Law $c\boldsymbol{E} = -\boldsymbol{v}\times\boldsymbol{B} + \eta\boldsymbol{\nabla}\times\boldsymbol{B}$

Diffusion coefficients σ, $Q = \boldsymbol{\nabla}\cdot(\kappa\boldsymbol{\nabla}T)$, η

Radiative properties $Q = -\boldsymbol{\nabla}\cdot(\boldsymbol{F}_{\mathrm{rad}})$

Constitutive relations are statements about the material properties of the medium (in this case, plasma). The choice of different constitutive relations spawns a diversity of MHD models.

A Diversity of MHD Models

Cheung & Isobe (2014)
Liv Rev Sol Phys

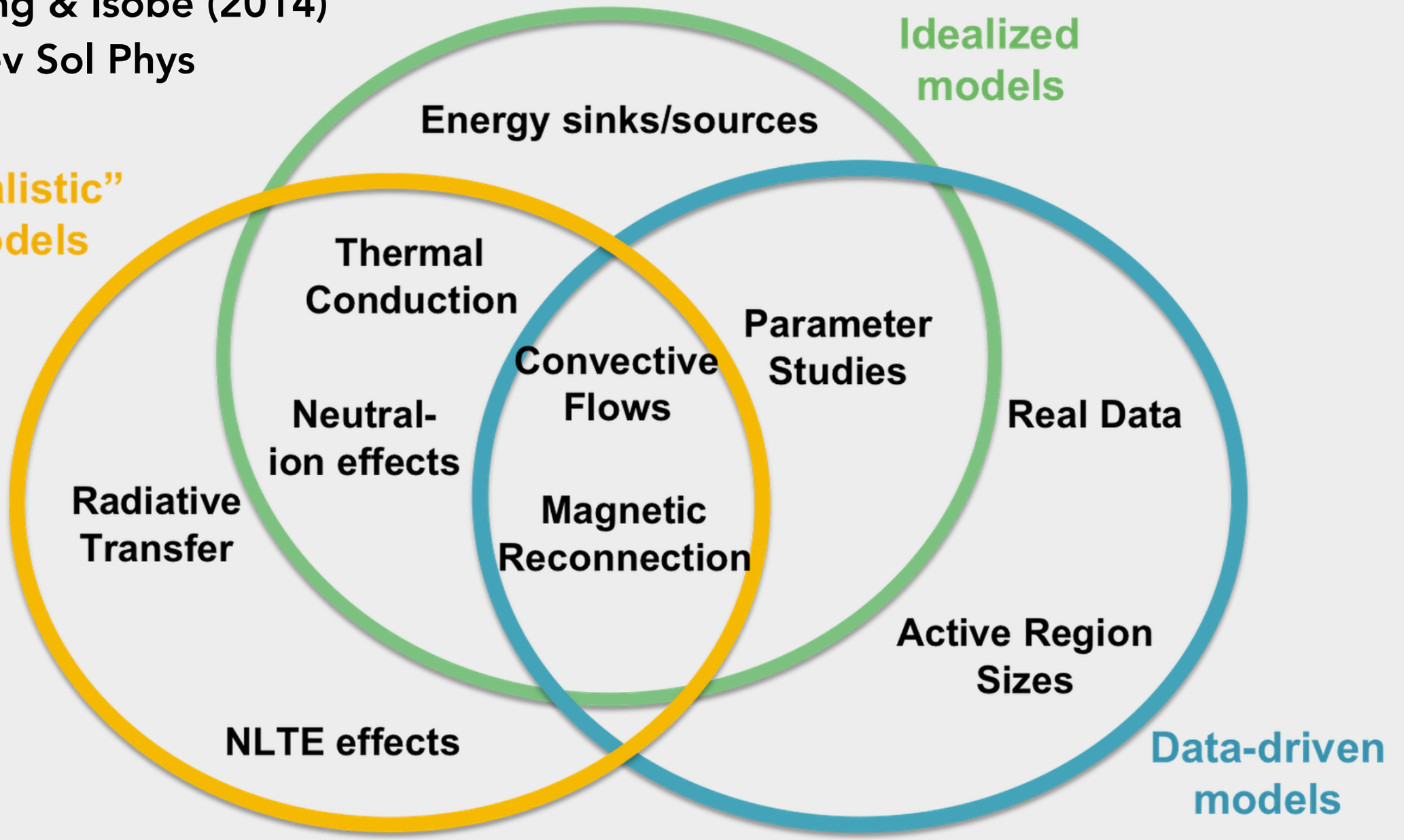

Figure 5: Models of magnetic flux emergence can be roughly divided into three categories, though there are large areas of overlap between them. So-called 'realistic' models attempt to include all the known important physical ingredients, while idealize models generally focus on studying a more limited set of effects. For case studies of certain observed emerging flux studies, data-driven models are used.

Science questions

- What are the appropriate constitutive relations in different parts of the solar atmosphere? Let's generalize this to:
  - What are the constitutive relations for different plasma regimes?
- Are there specific conditions that determine the onset of reconnection?
- Can we put constraints on reconnection theory? Is there evidence for tearing mode instabilities in current sheets leading to hierarchical plasmoid formation (Shibata & Tanuma 2001)?
- How is the released magnetic energy channeled into other forms, and what are the observational consequences?

Science questions

- Are solar flares and eruptions triggered by small-scale disturbances?
- What does the chromospheric magnetic field look like before an eruption/flare?
- How important are ion-neutral, and more generally, multi-fluid effects?
- How does MHD wave mode conversion occur along magnetic channels and at the boundaries of magnetic domains?

Magnetic Field Diagnostics of Emerging Flux

Extremely large volume of papers studying photospheric magnetic observations of flux emergence.

Ground-based instruments: Leka et al. (1996); Strous et al. (1996); Lites, Skumanich & Martinez Pillet (1998); Strous & Zwaan (1999); De Pontieu (2002); **Kubo, Shimizu & Lites (2003)**; Watanabe et al. (2008, 2011); Guglielmino et al (2010); Schlichenmaier et al. (2010), Yurchyshyn et al. (2010), Rutten et al. (2013), Lim et al. (2016),

Balloons: Flare Genesis Experiment Bernasconi et al. (2002); **Pariat et al (2004)**

SUNRISE Guglielmino et al. (2012)

MDI Many many many papers

Hinode **Centeno et al. (2007)**; Cheung et al. (2008); Okamoto et al. (2008); Magara (2008); Gonzalez & Bello Rubio (2009); Otsuji et al. (2009, 2011); Ishikawa, Tsuneta & Jurčák (2010), Shimizu, Ichimoto & Suematsu (2012)

SDO/HMI Centeno et al (2012): Liu & Schuck (2012); Toriumi, Hayashi & Yokoyama (2012, 2014); Tarr & Longcope (2012); Cheung & DeRosa (2012), Cheung et al. (2015)

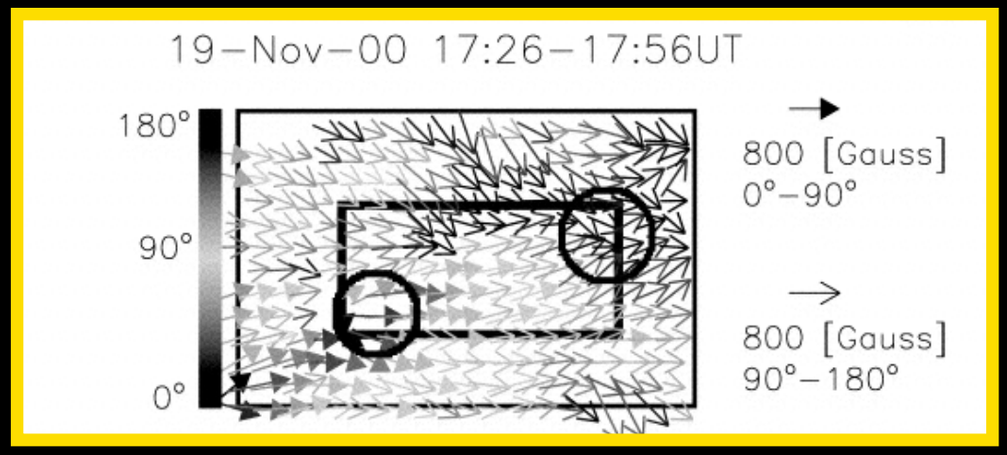

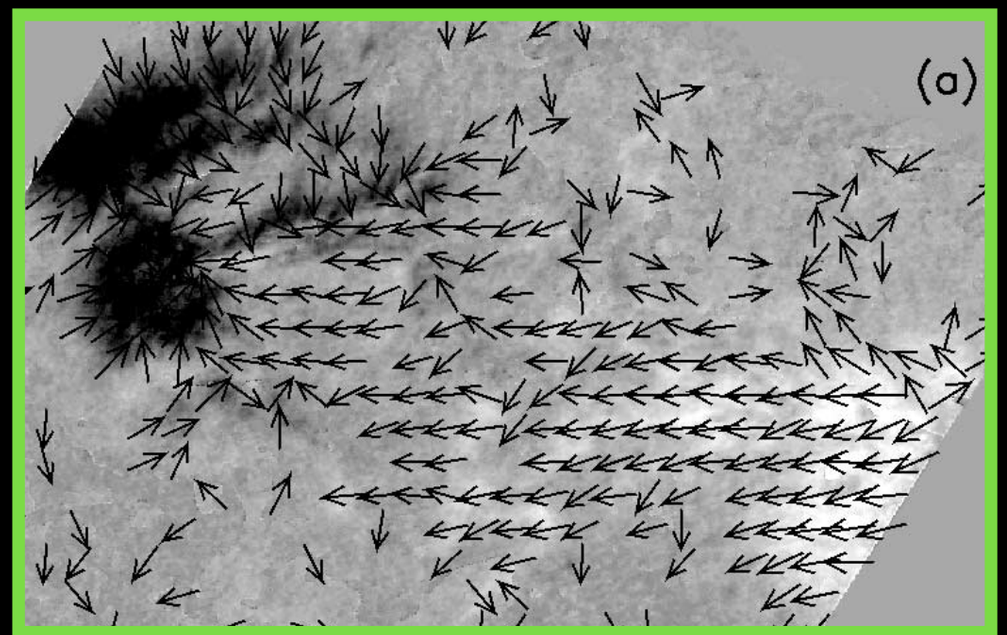

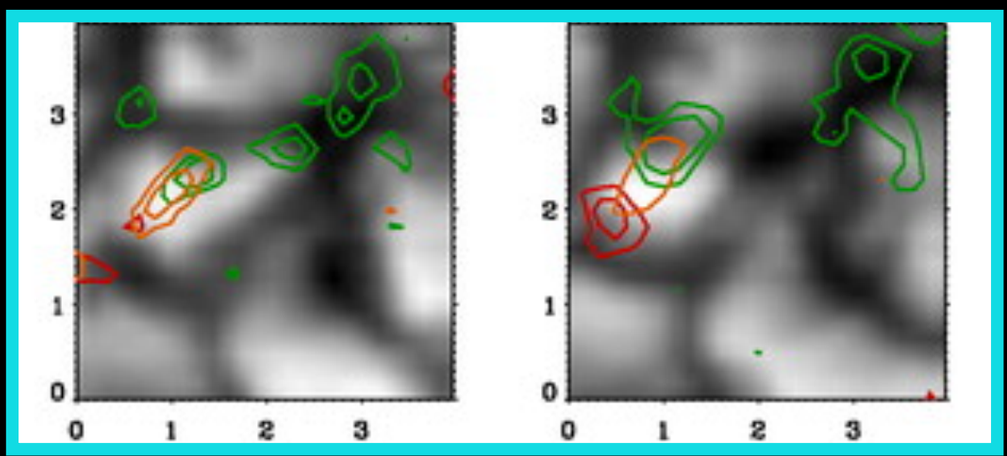

1-4 1-5 1-10 1-11 1-12 2-3 2-4 2-5 2-13 2-14 2-15 2-16 2-17 2-24 2-25 2-26

350
field strength (G)
0
(420km)
-3.0
-2.5
-2.0
-1.5
-1.0
-0.5
0.0
log τ

upflow
-3.0
Doppler velocity (km/s)
+3.0
downflow
(420km)
-3.0
-2.5
-2.0
-1.5
-1.0
-0.5
0.0
log τ

normarized continuum intensity
1.2
1.1
1.0
0.9
0.8

600km

1320km

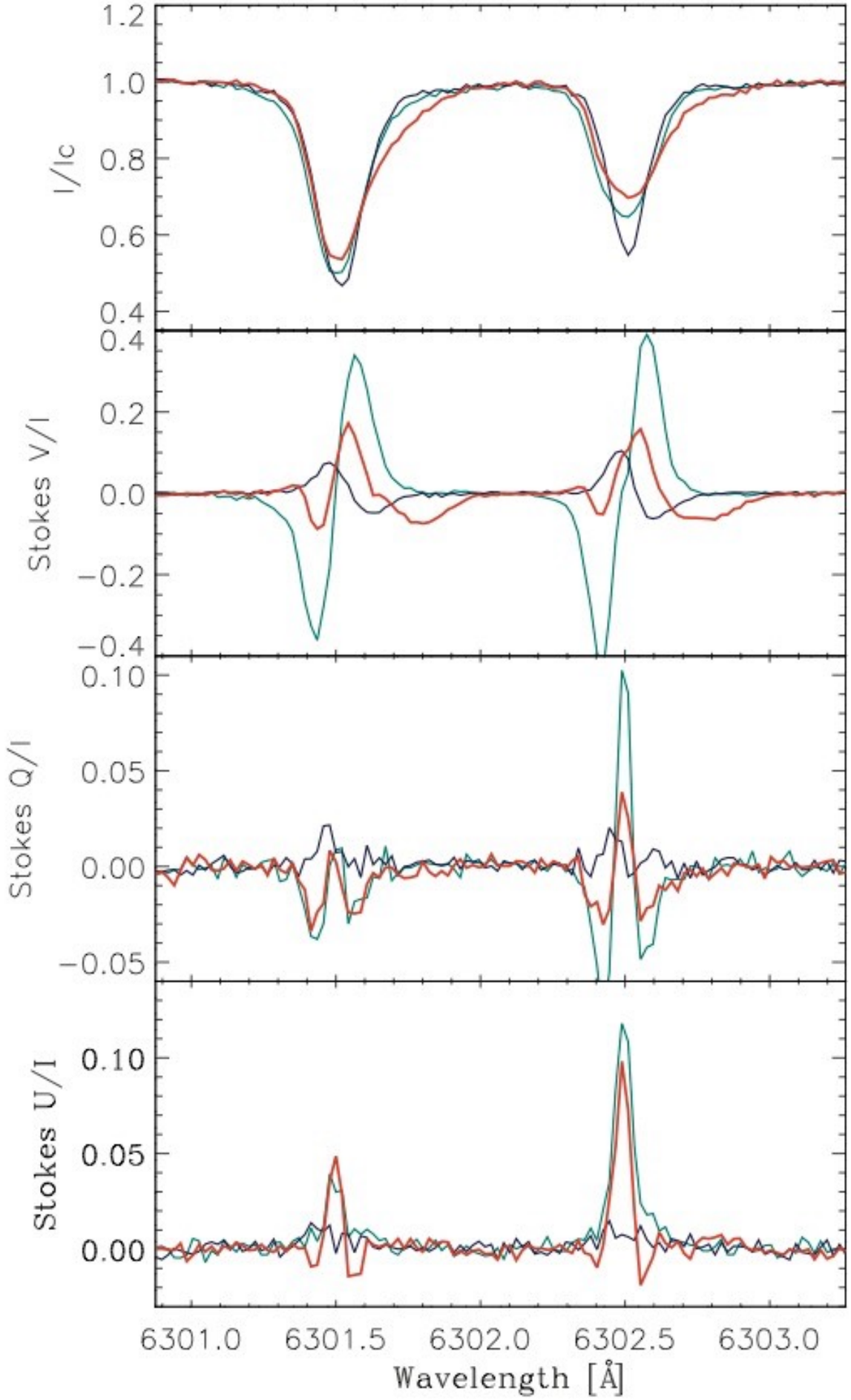

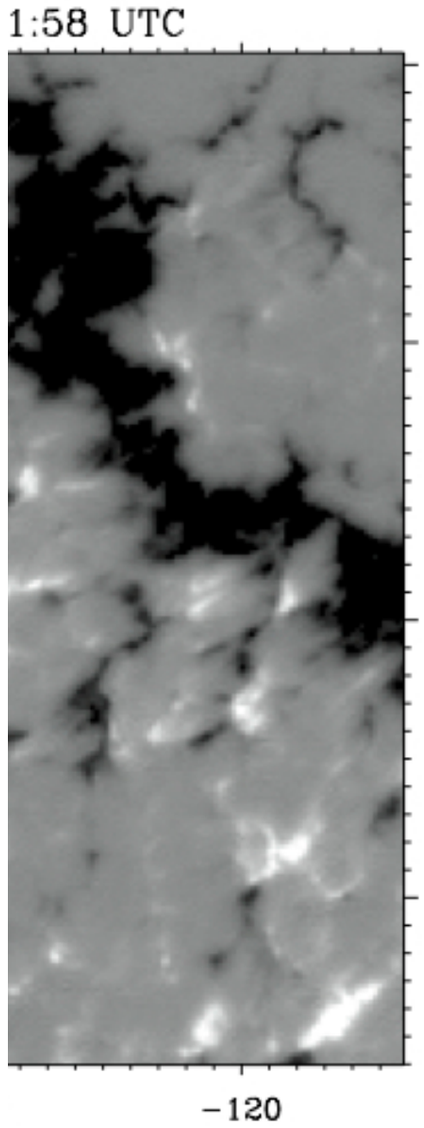

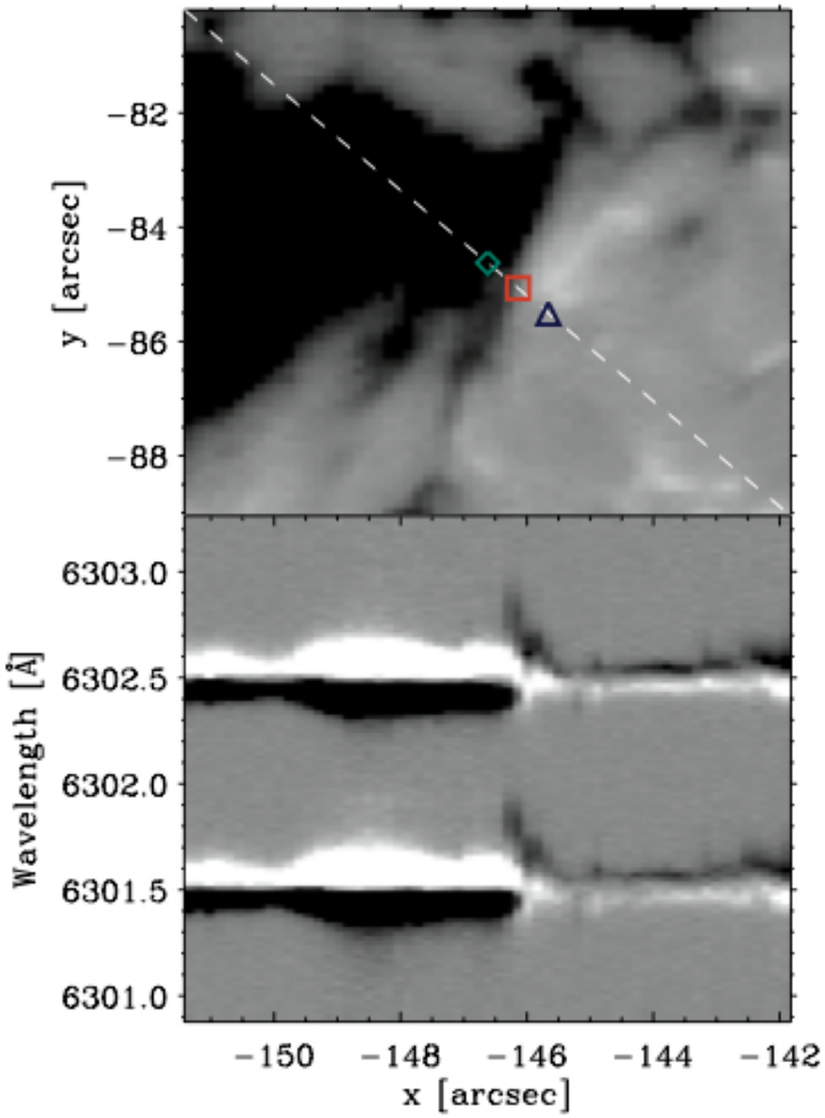

Supersonic downflows in a flux cancellation site (Cheung et al. 2008) from Hinode/SP. Perhaps a signature of reconnection down flows.

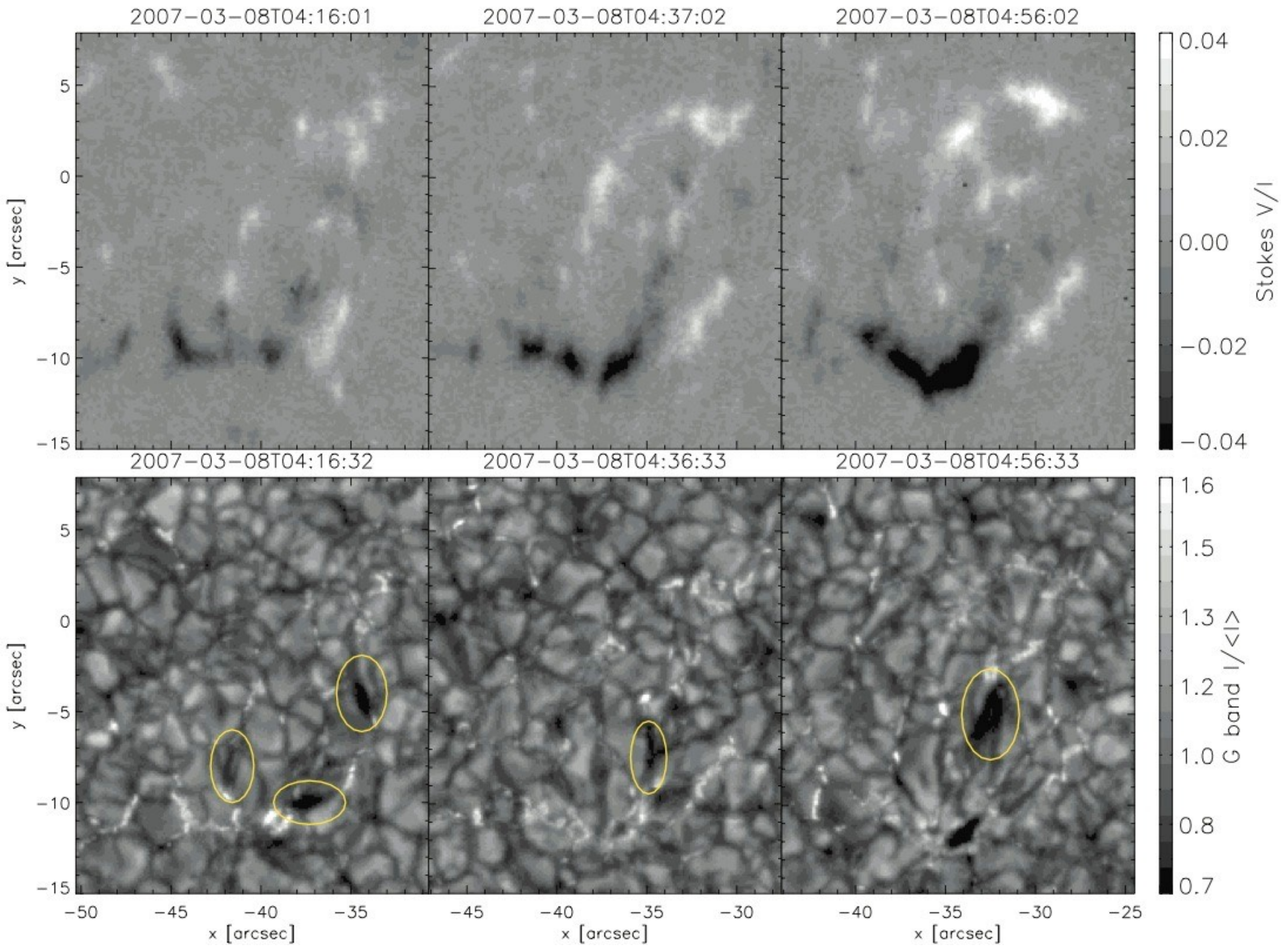

From Cheung et al. (2008): SOT/NFI observations of dark lanes in emerging flux regions.
See also Strous & Zwaan (1999).

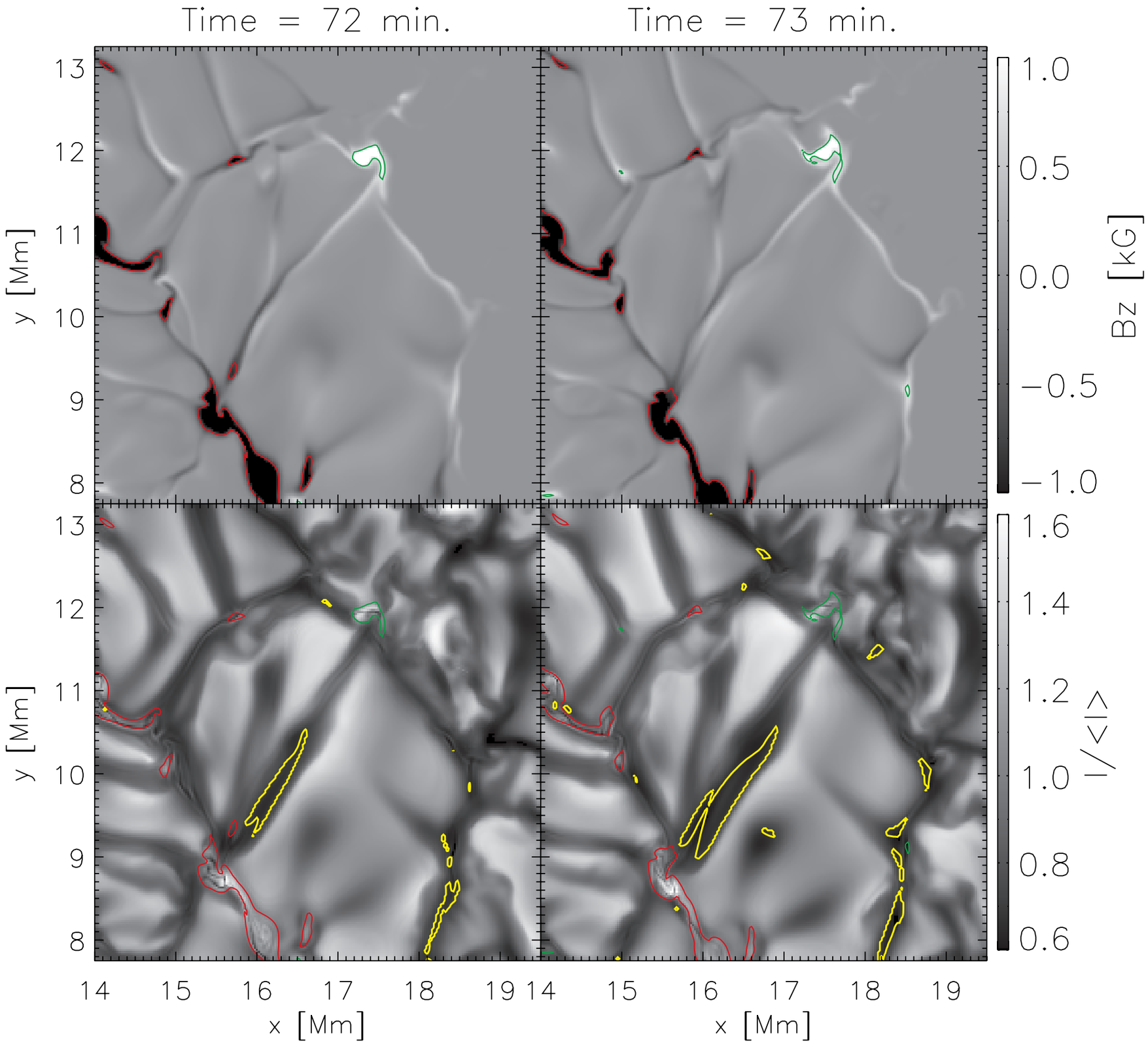

From Cheung et al. (2008): Radiative MHD simulation of emerging flux reproduces dark lanes. Basically, upflow regions with low entropy.

Flux emergence in the photosphere

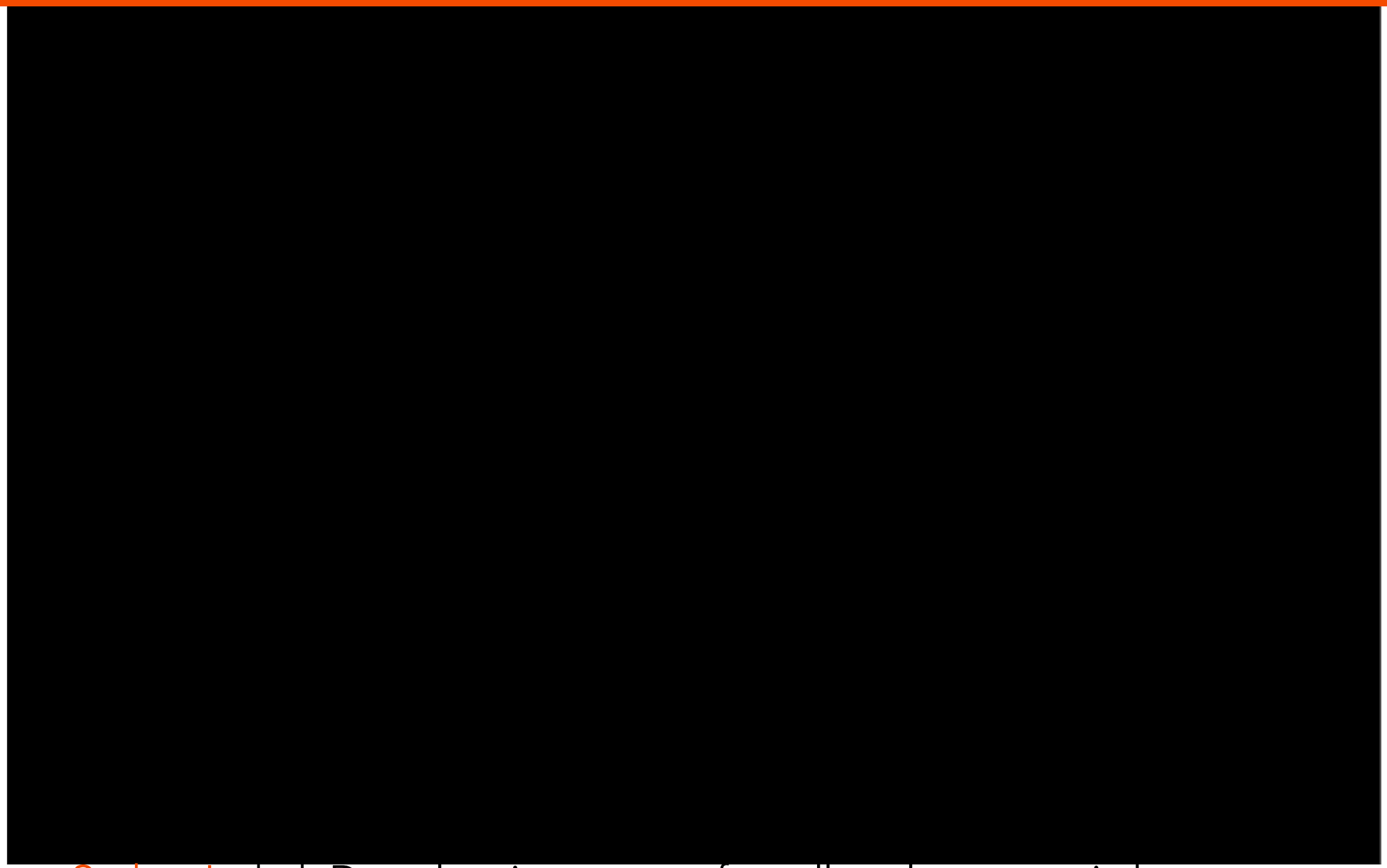

- Stokes I: dark Doppler signatures of small-scale magnetic loops.
- Stokes Q & U: elongated features in the body of the loop.
- Stokes V: most of the signal is concentrated at the footprints of the loops.

Slide credit: J. De La Cruz Rodriguez

Magnetic bubbles in the photosphere

SST/CRISP - Ca II 8542

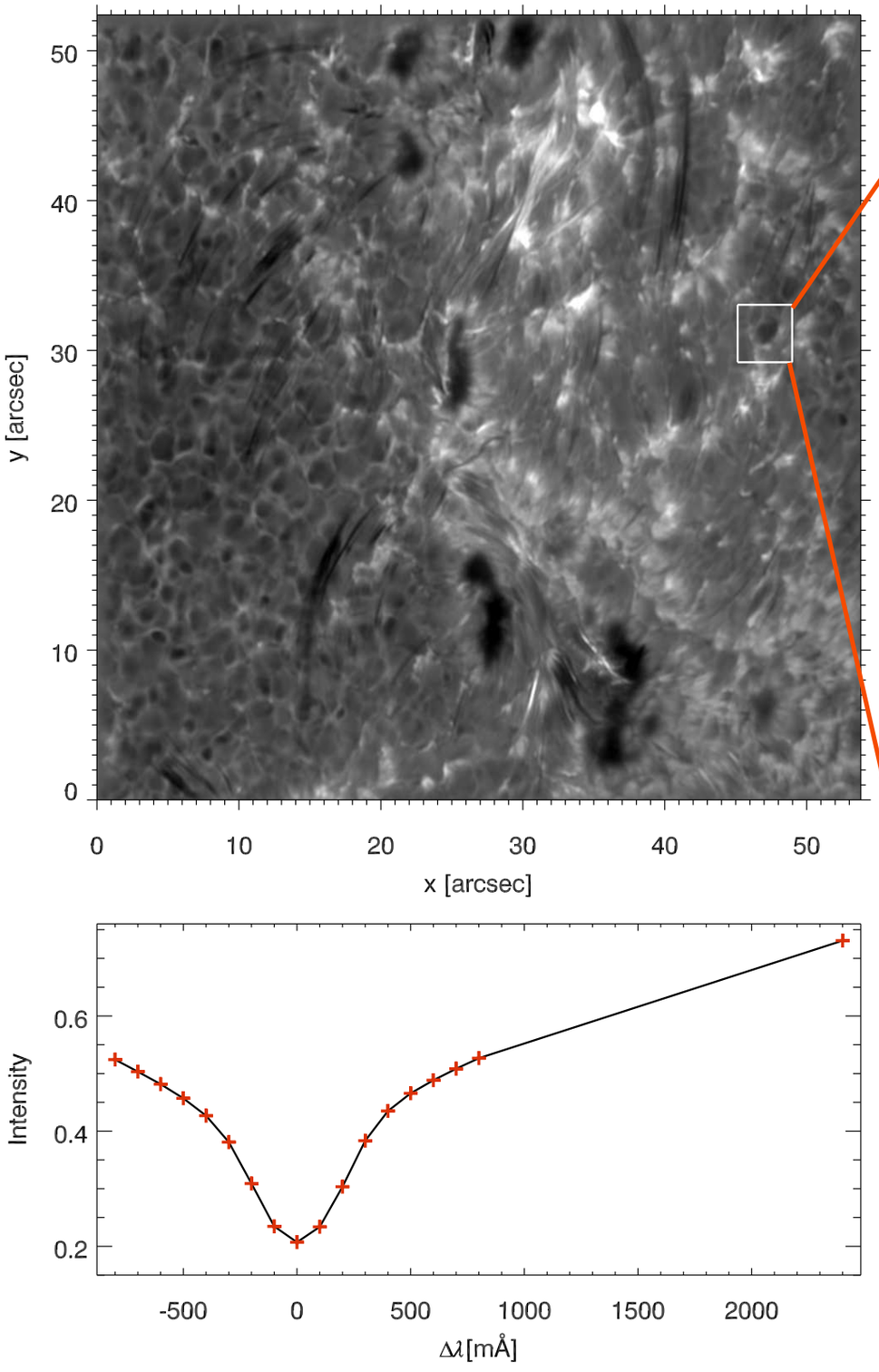

SST/CRISP - 6302, full-Stokes

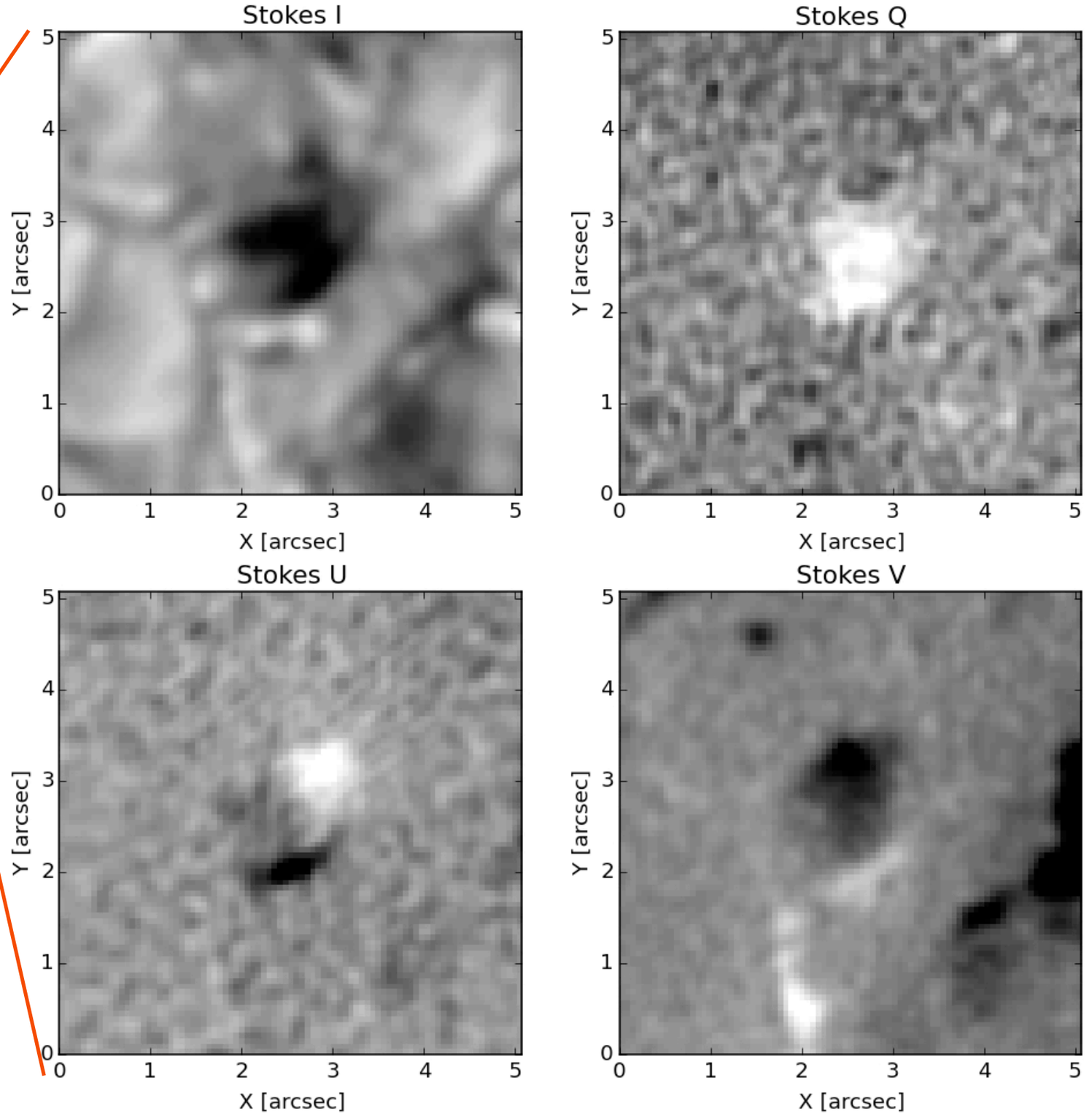

Slide credit: J. De La Cruz Rodriguez

Ortiz et al. (2014)

Magnetic bubbles in the chromosphere

SST/CRISP - 8542

Ortiz et al. (2014); de la Cruz Rodríguez et al. (2015)

From Ortiz et al. (2014):

- The emergence is not visible at line center in Ca II 8542, during our series.
- Canopy of fibrils above the emerging flux in the chromosphere.
- Line positions along the wing show similar dark features as in the Fe I lines.
- Observed delay in 8542 relative to Fe I 6302.
- No signal in Stokes Q & U, very weak Stokes V signal.
- See Martinez-Sykora et al. (2008, 2009) for Bifrost models [this bullet point added by M. Cheung].

Slide credit: J. De La Cruz Rodriguez

De la Cruz Rodriguez et al. (2015): non-LTE Stokes inversion of SST Ca II 8542 Å observations of an emerging magnetic bubble.

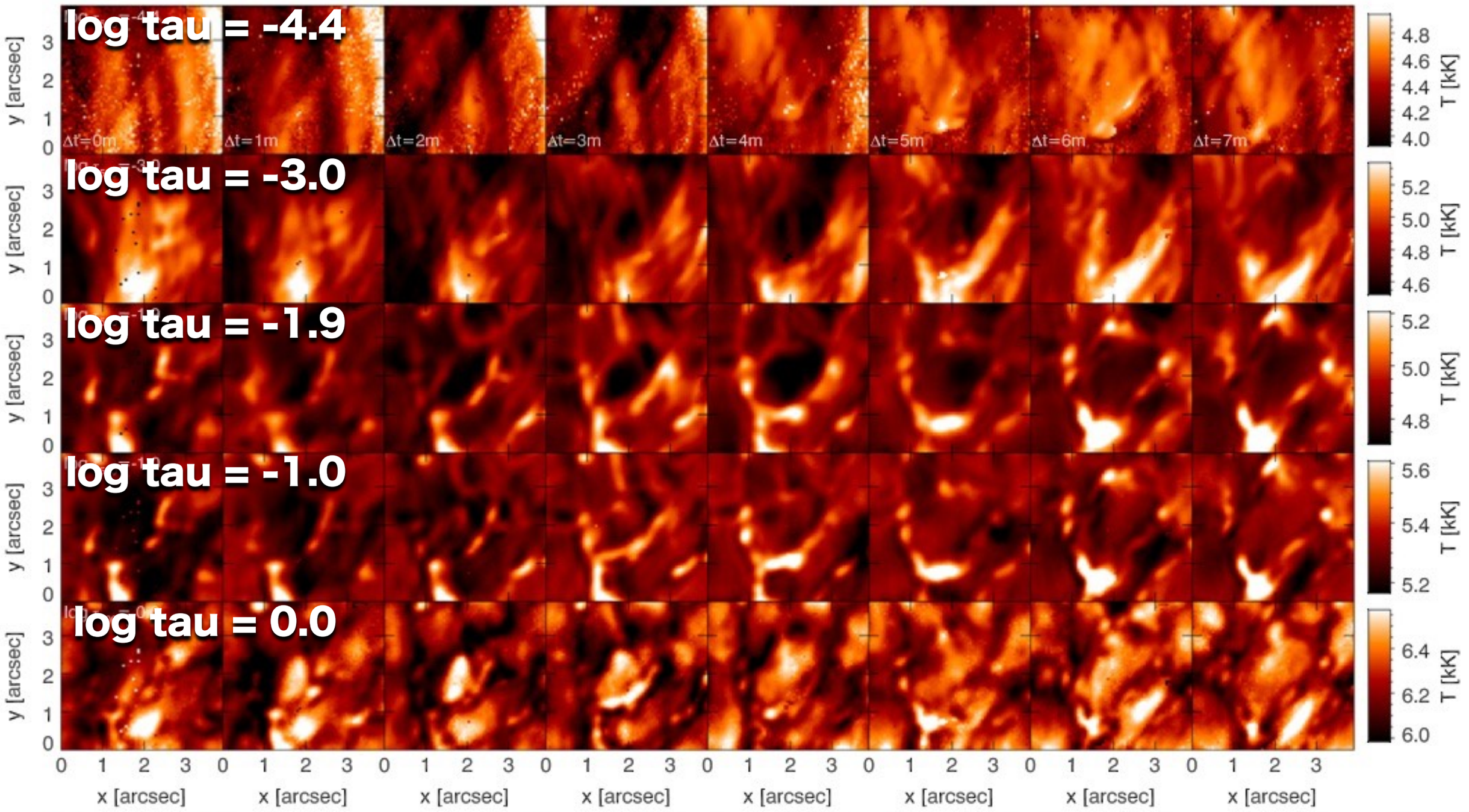

Figure 2. Temporal evolution of the temperature inferred with a non-LTE inversion. From left to right, the panels show consecutive time steps from our time series. From bottom to top, the panels illustrate the inferred temperature at iso-log τ_{500} surfaces in the model. $\Delta t = 0$ corresponds to 10:07:16 UT.

Above: Sequence of temperature maps at 1 min cadence

Below: Sequence of Doppler velocity maps at 1 min cadence

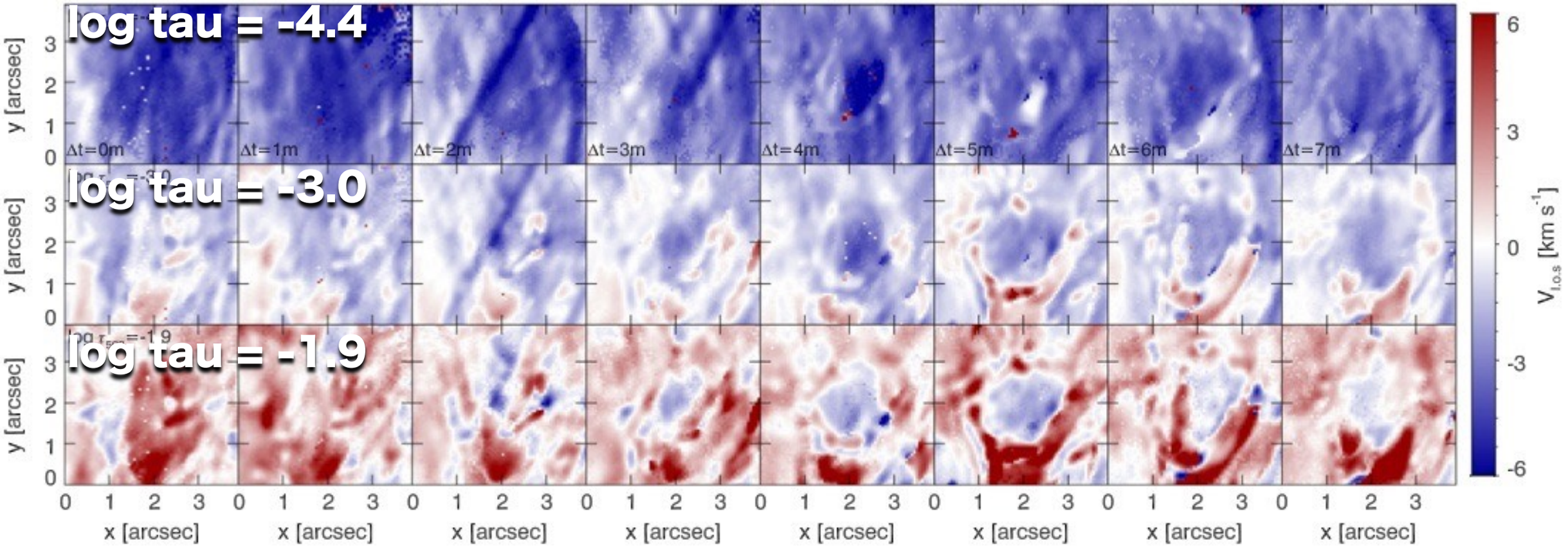

Figure 3. Temporal evolution of the line-of-sight velocity inferred with a non-LTE inversion. From left to right, the panels show consecutive time steps from our time series. From bottom to top, the panels illustrate the inferred temperature at iso-log τ_{500} surfaces in the model. $\Delta t = 0$ corresponds to 10:07:16 UT.

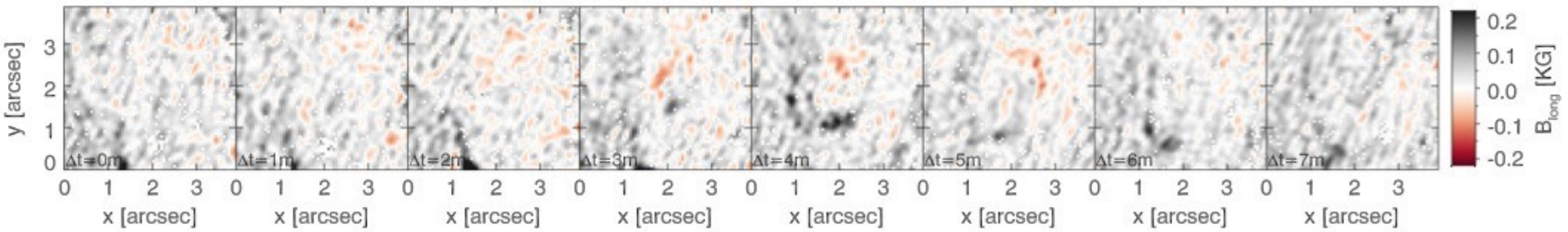

Figure 4. Temporal evolution of the longitudinal component of the magnetic field inferred with a non-LTE inversion. From left to right, the panels show consecutive time steps from our time series. $\Delta t = 0$ corresponds to 10:07:16 UT.

Above: Sequence of Bz maps at 1 min cadence

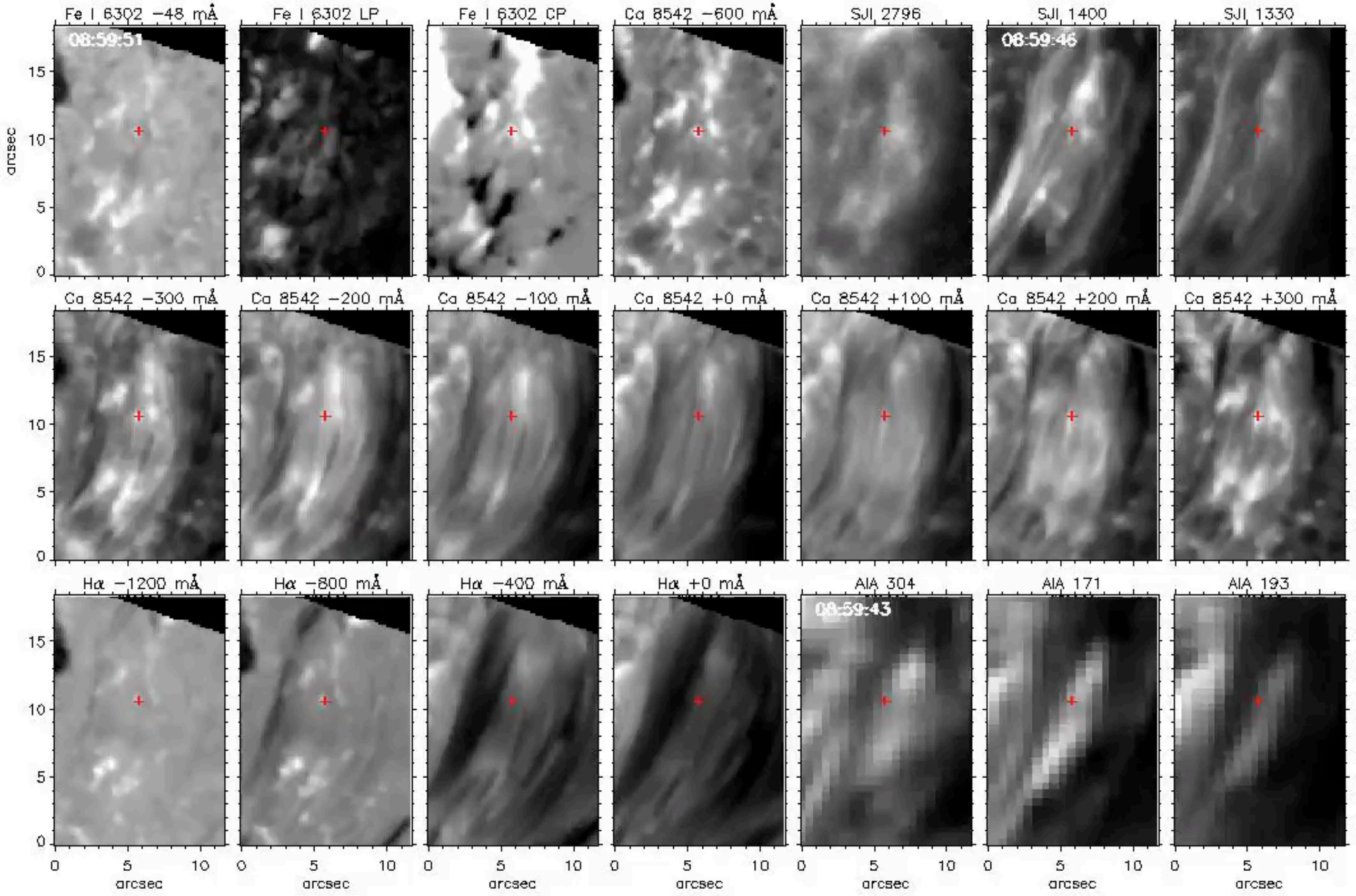

Ortiz et al. 2016

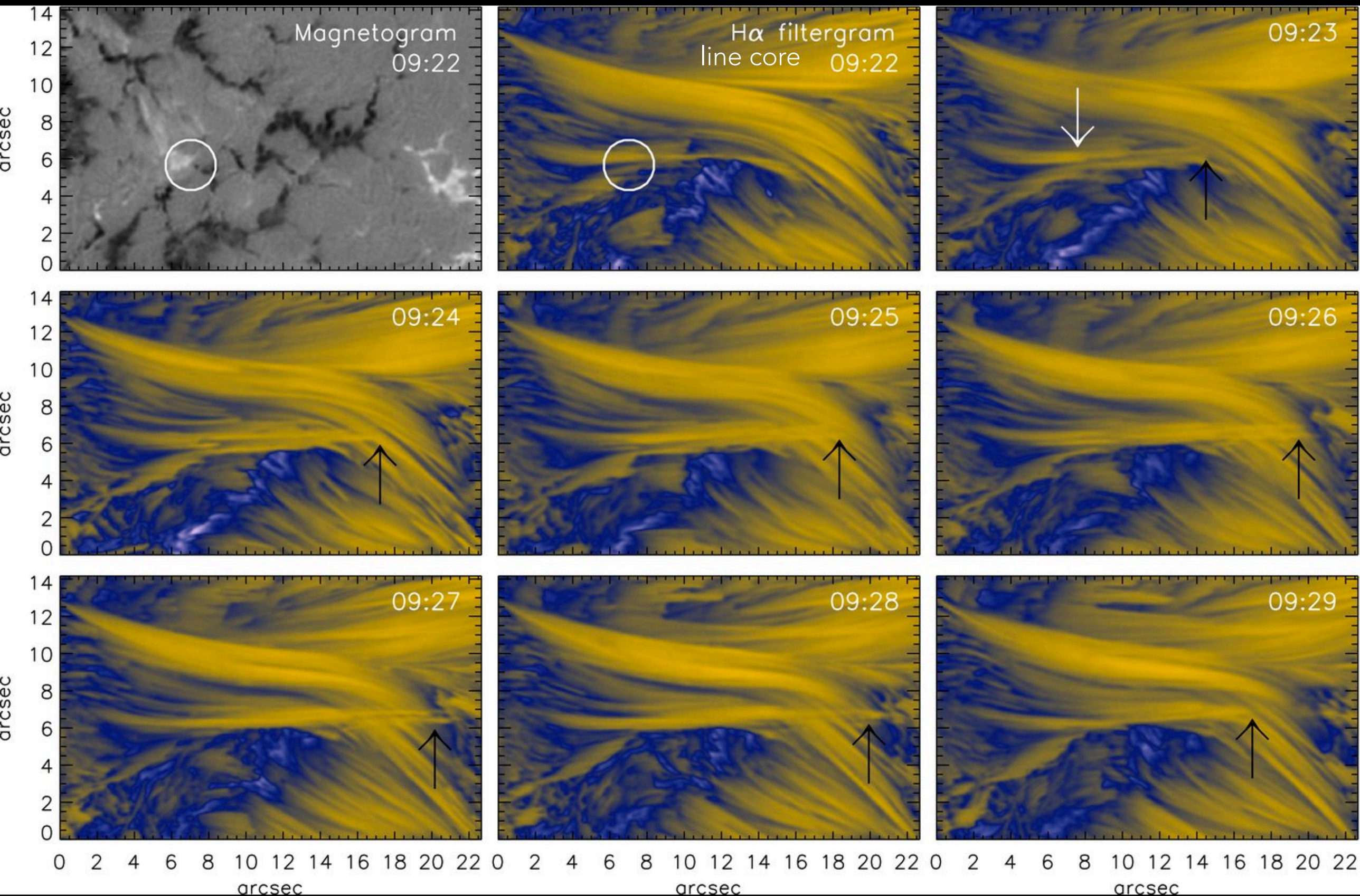

Guglielmino et al. (2010) - chromospheric surge in EFR observed with SST

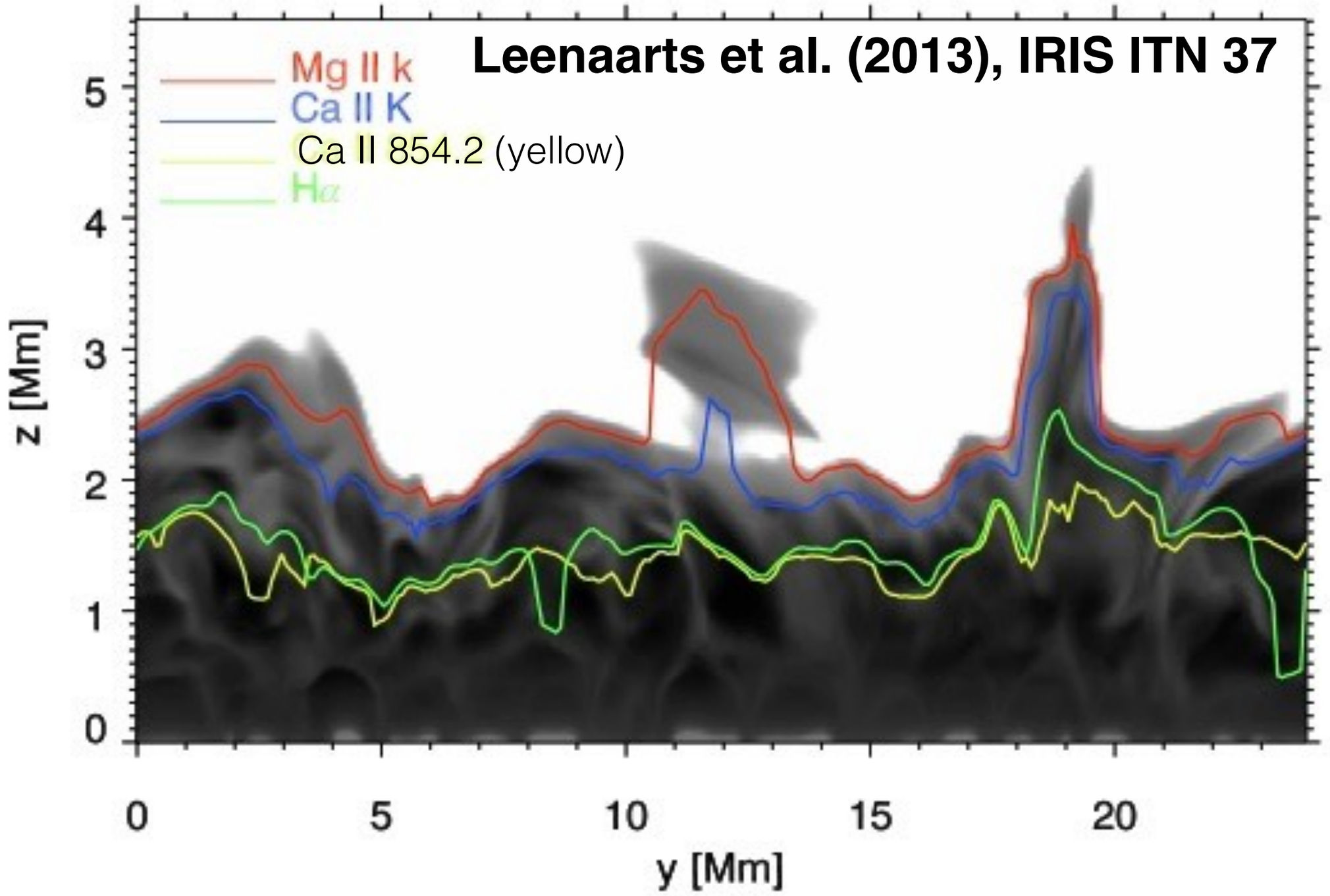

Figure 1. Differences between $\tau = 1$ heights of Mg II k, Ca II K, Ca II 854.2 nm, and Hα in an yz-slice of the 3D model atmosphere. The image displays the temperature, clipped at 20 kK, with curves of the maximum $\tau = 1$ height of the various lines overplotted.

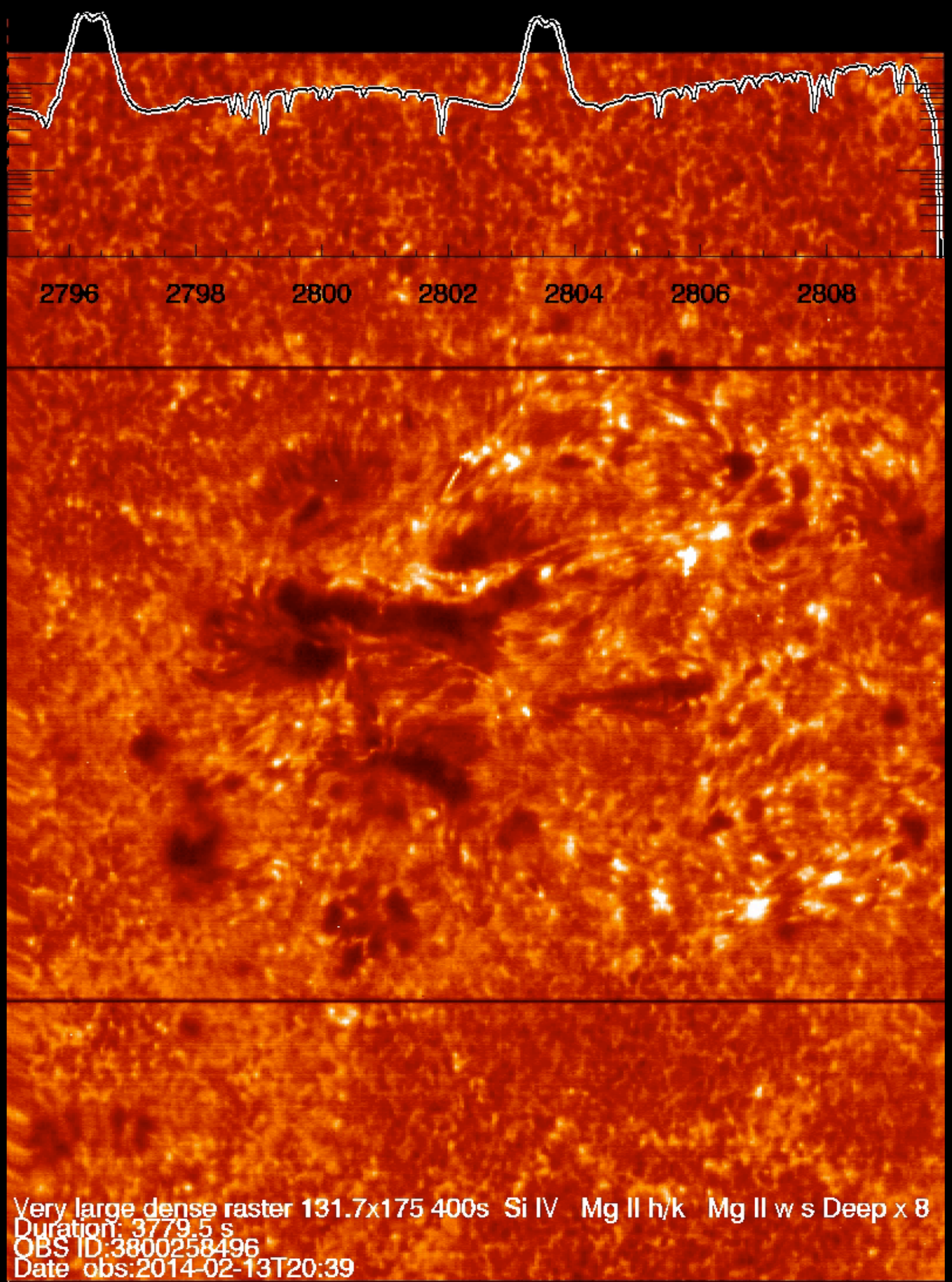

IRIS raster scan of an EFR: Mg II k and Mg II triplet

Scanning from the wing to the k3 (core), one sees the transition from reversed granulation to arch filaments / fibrils.

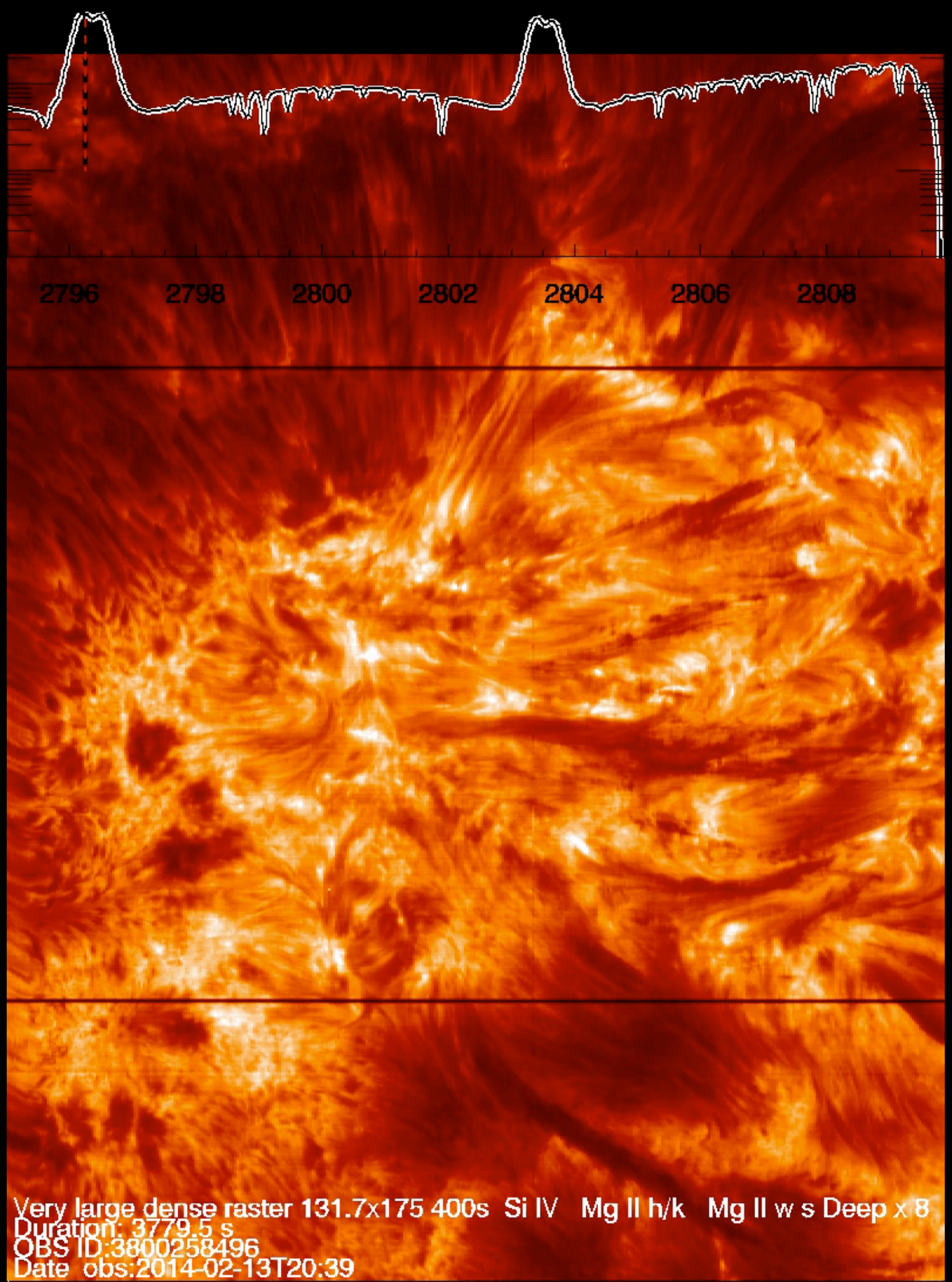

IRIS raster scan of an EFR: Mg II k and Mg II triplet

Scanning from the wing to the k3 (core), one sees the transition from reversed granulation to arch filaments / fibrils.

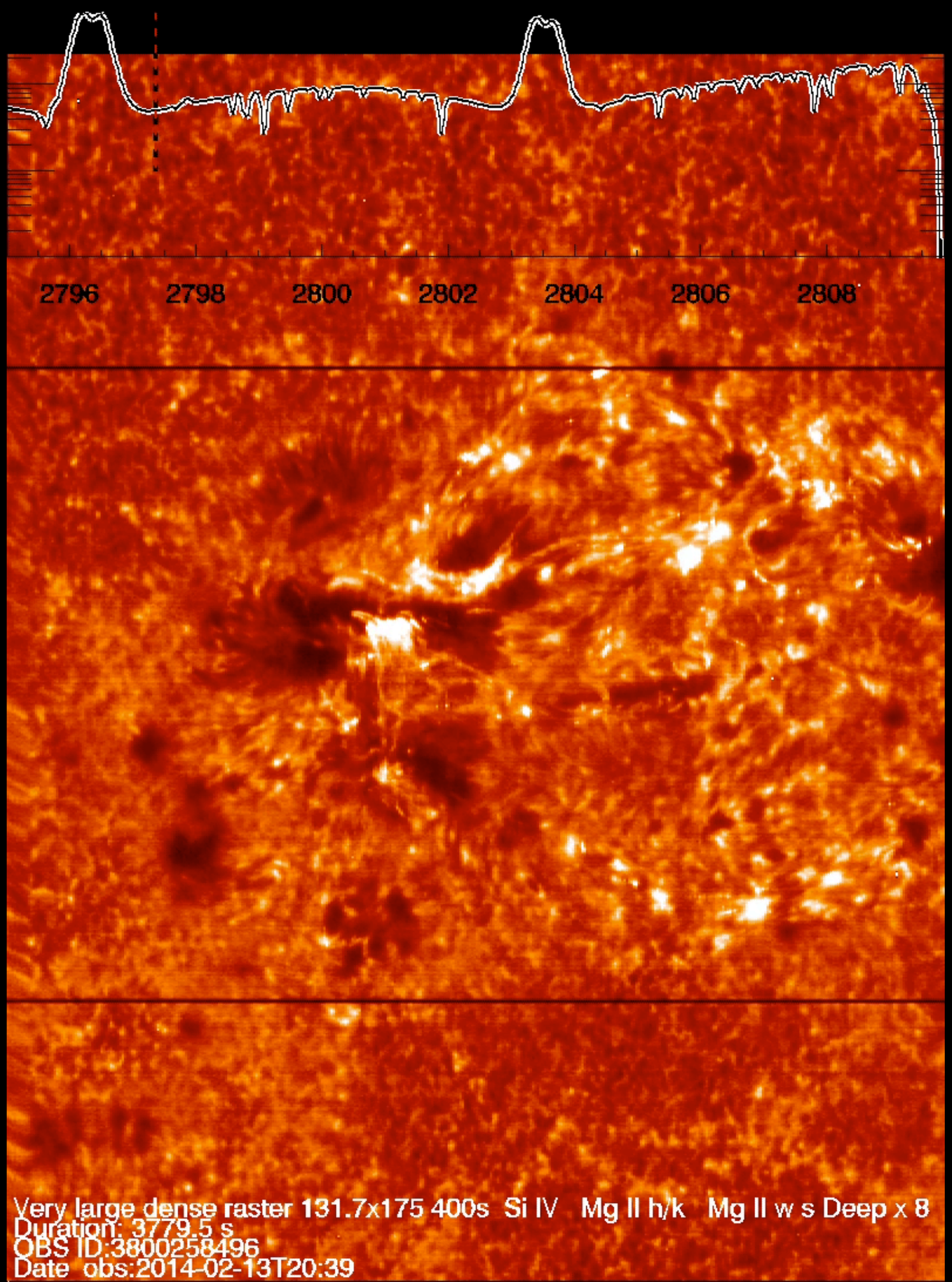

IRIS raster scan of an EFR: Mg II k and Mg II triplet

Scanning from the wing to the k3 (core), one sees the transition from reversed granulation to arch filaments / fibrils.

Scanning to the Mg II triplet, one sees different structure in the chromosphere (seemingly lower lying loops).

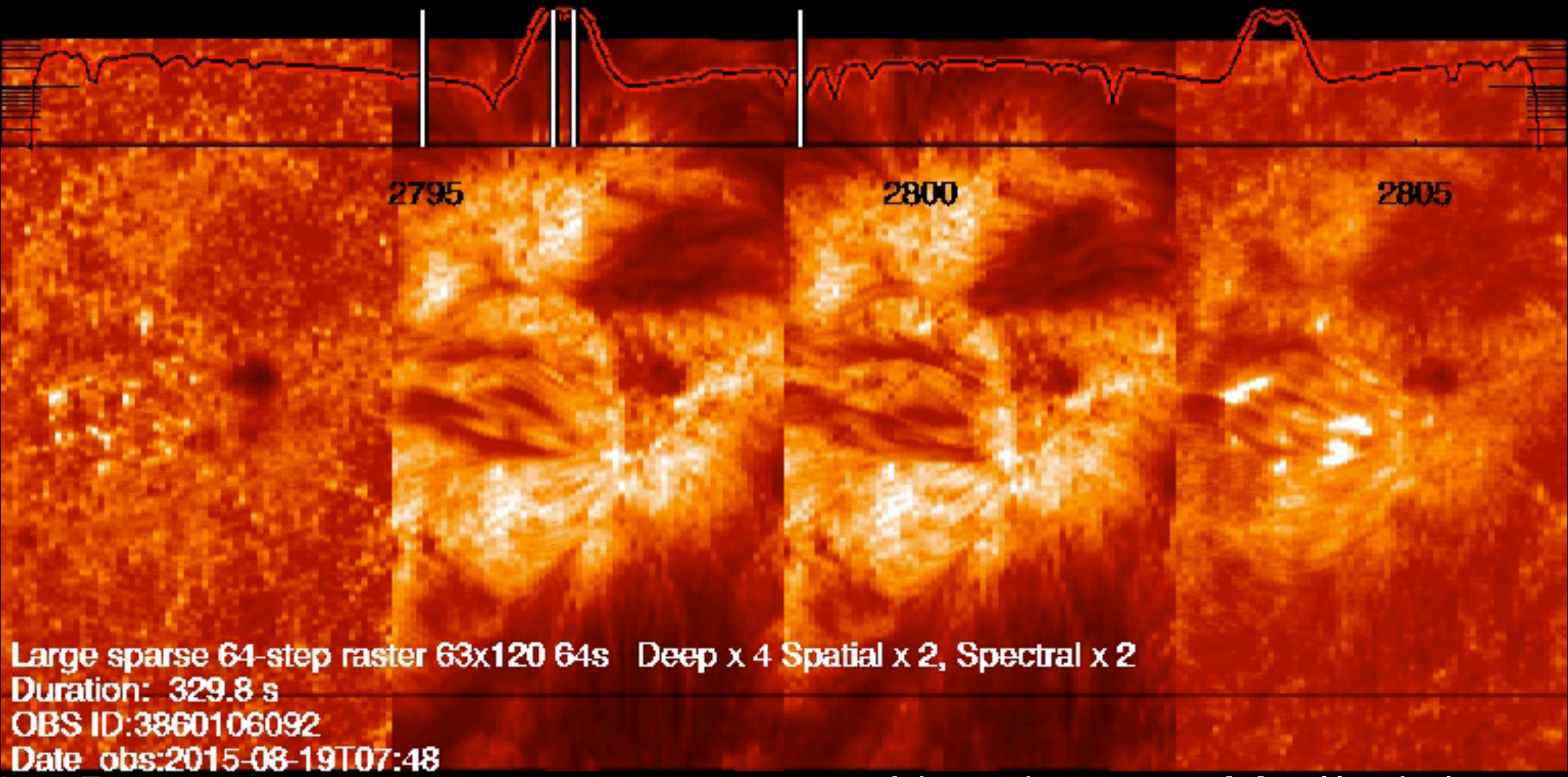

Blue wing Near k2v Near k2r Mg II triplet

IRIS Mg II rasters of an EFR @ 330s cadence

Mg II triplet lines are a diagnostics for low chromospheric heating (Pereira et al. 2015)

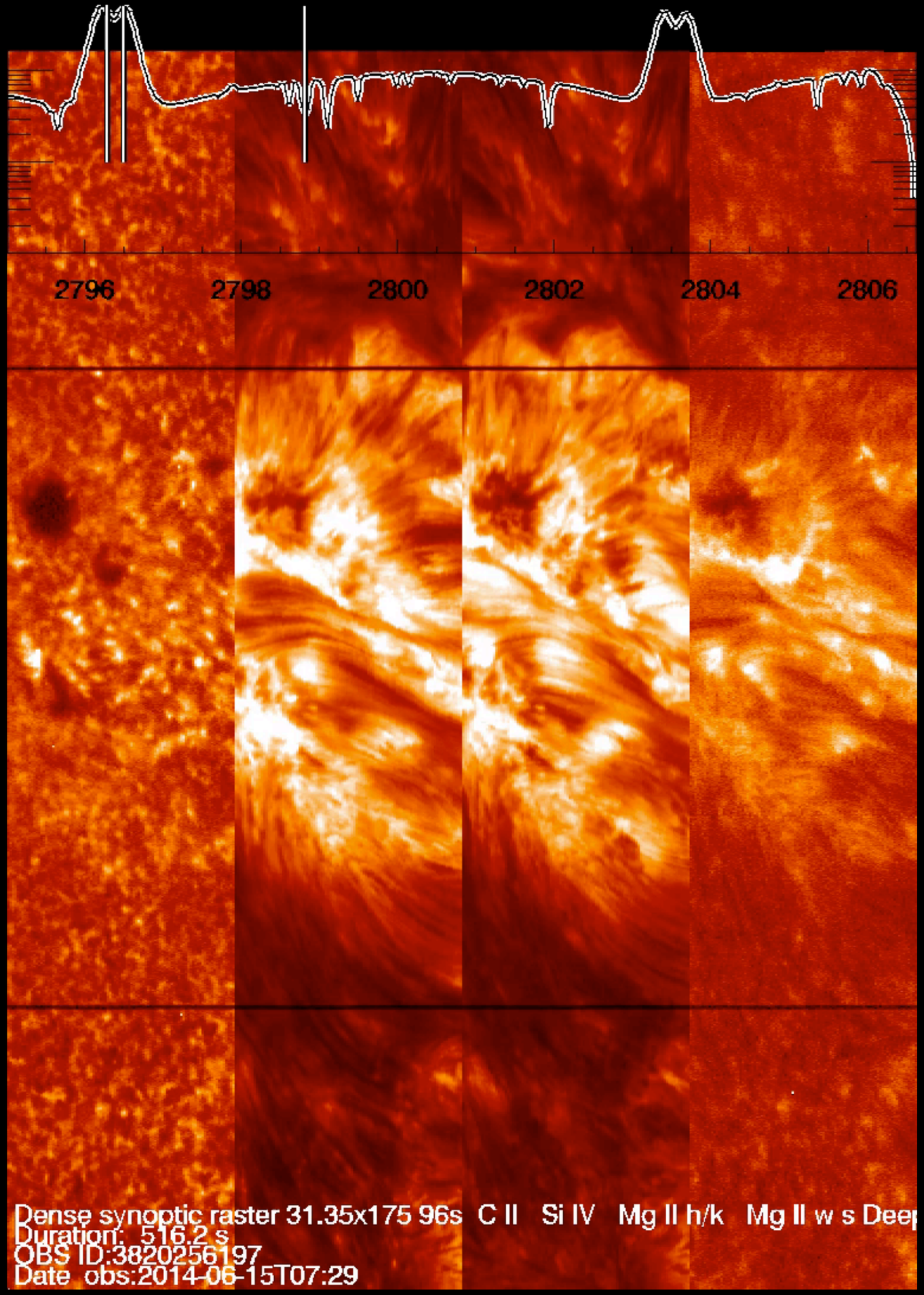

Wouldn't it be fantastic to put magnetic field vectors on these images?

NASA Heliophysics Grand Challenges Research (HGCR): Physics and Diagnostics of the Drivers of Solar Eruptions






Radiative MHD simulations of AR eruptions

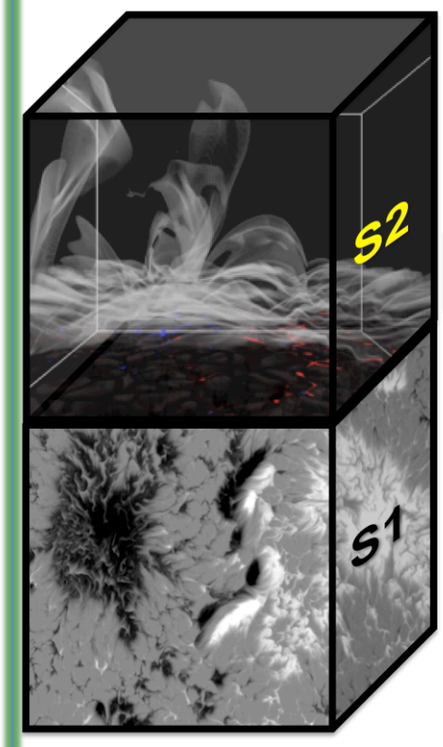

Forward synthesis of observables

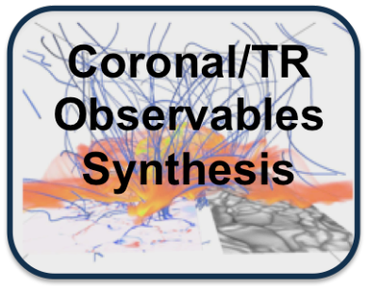

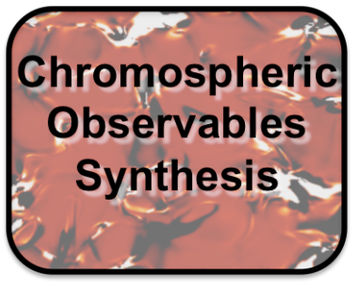

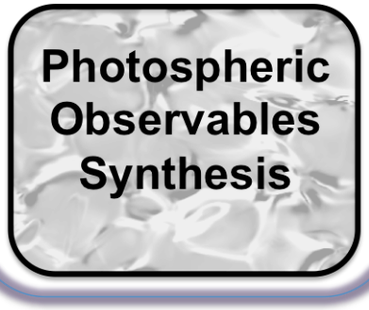

Understand driver(s) of solar eruptions

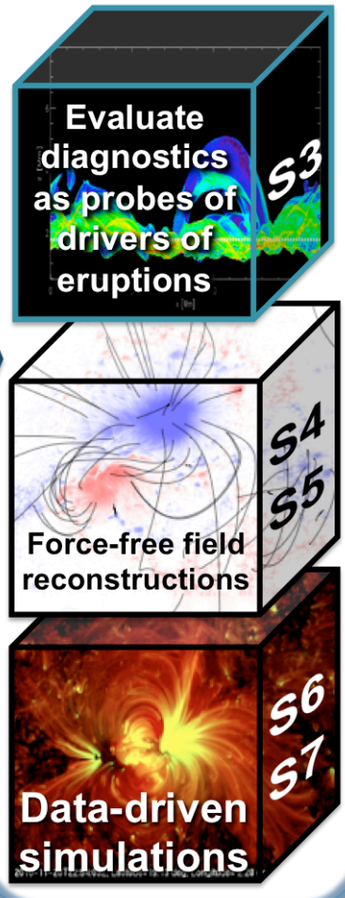

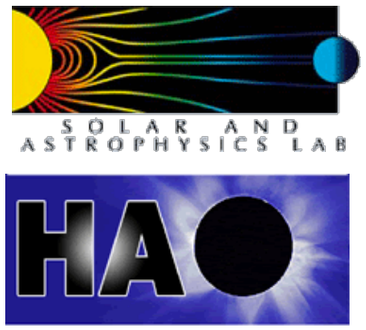

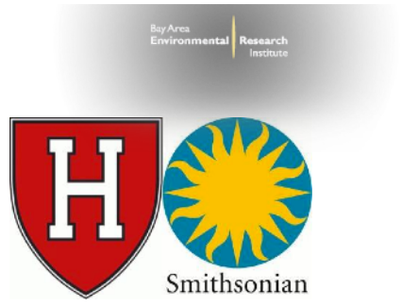






A collaboration between LMSAL (PI: Cheung), HAO, BAERI, SAO & U Oslo, supported by NASA Grant NNX14AI14G

Radiative MHD simulation of AR formation* (M. Rempel)

*work done for NASA's Heliophysics Grand Challenges Research project (LMSAL/NCAR/SAO/BAERI/U Oslo)

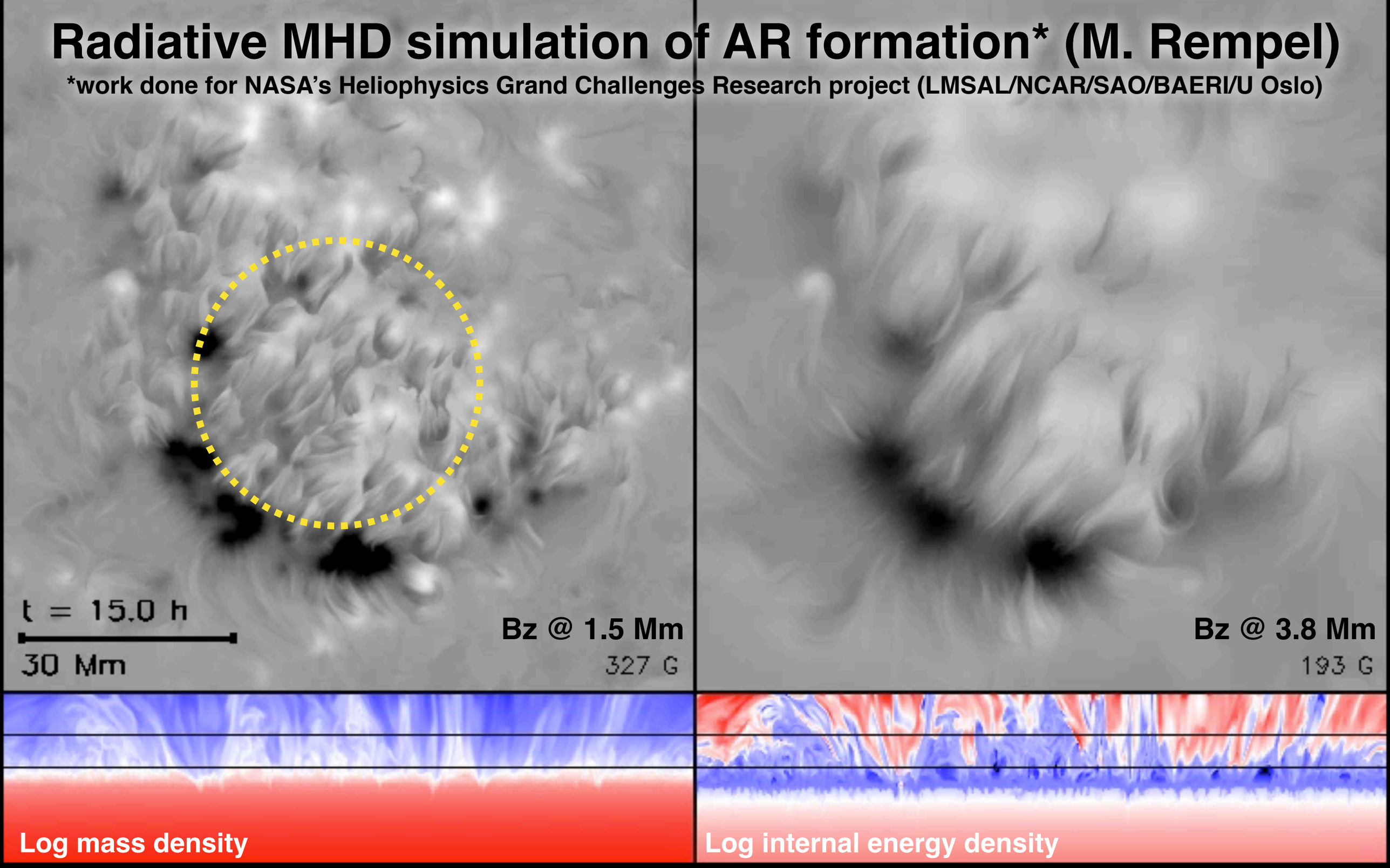

Integral Field Spectropolarimetry (e.g. DKIST, EST)

It would be an amazing achievement to map the chromospheric field to see reconnection in action.

Bz @ 1.5 Mm

1 arcmin
diameter FOV

IFU with 48x48
sample positions
spaced at 0.89 arcsec

Bz @ 1.5 Mm

1 arcmin
diameter FOV

IFU with 48x48
sample positions
spaced at 0.89 arcsec

Bz @ 1.5 Mm

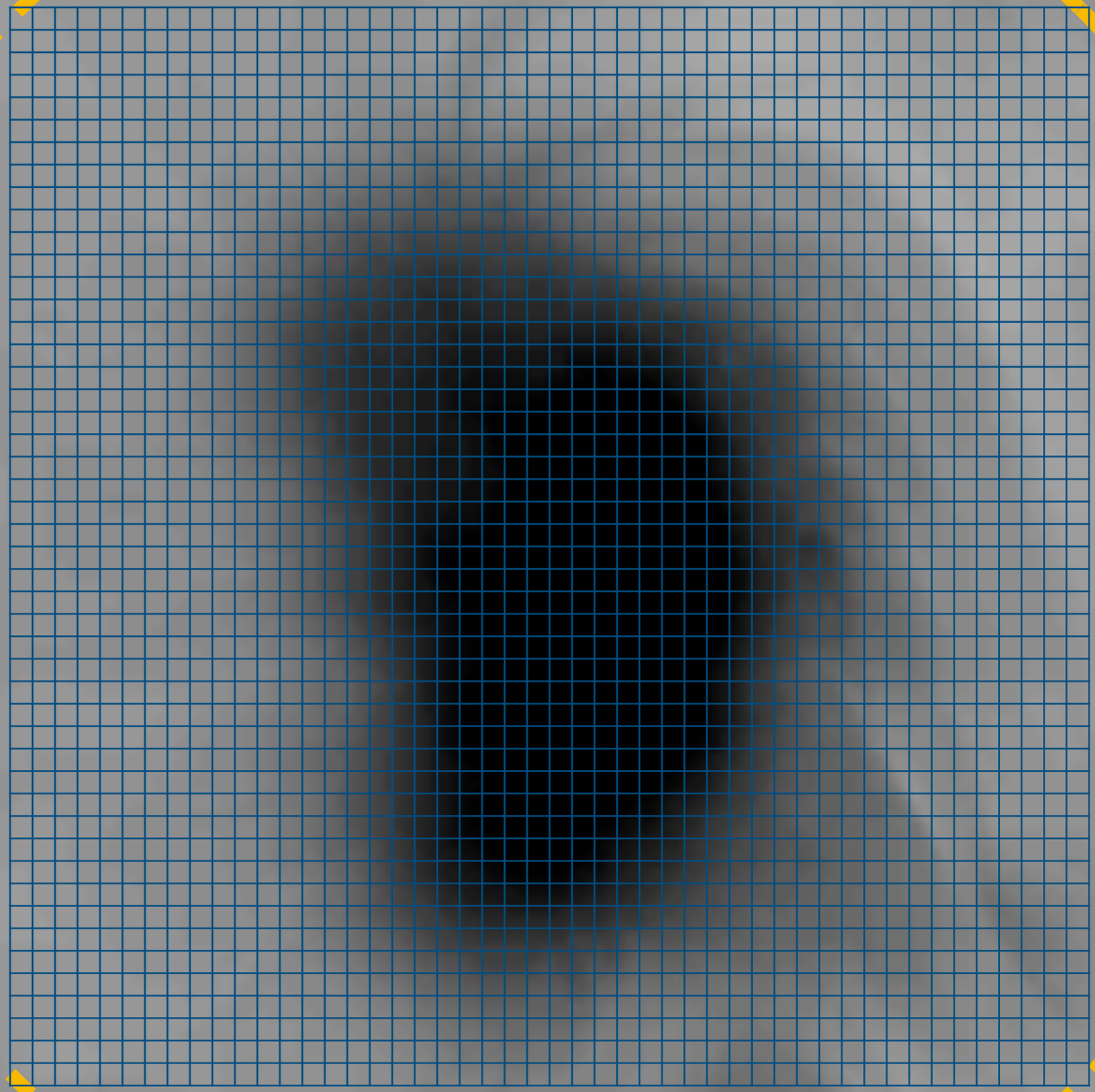

1 arcmin
diameter FOV

IFU with 48x48
sample positions
spaced at 0.89 arcsec

Data-Driven Simulations

SDO/AIA 94 @ 2013-07-21T12:34:01

SDO/AIA 94 @ 2013-07-21T13:28:49

SDO/AIA 94 @ 2013-07-21T14:15:13

SDO/AIA 94 @ 2013-07-21T16:18:25

IRIS

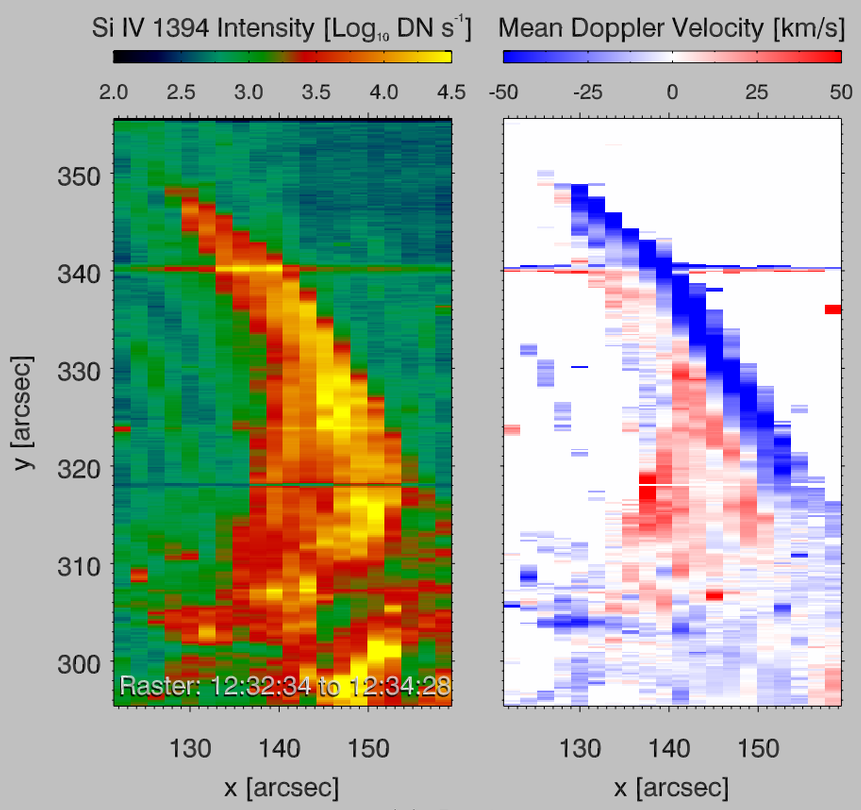

(a) Jet 1

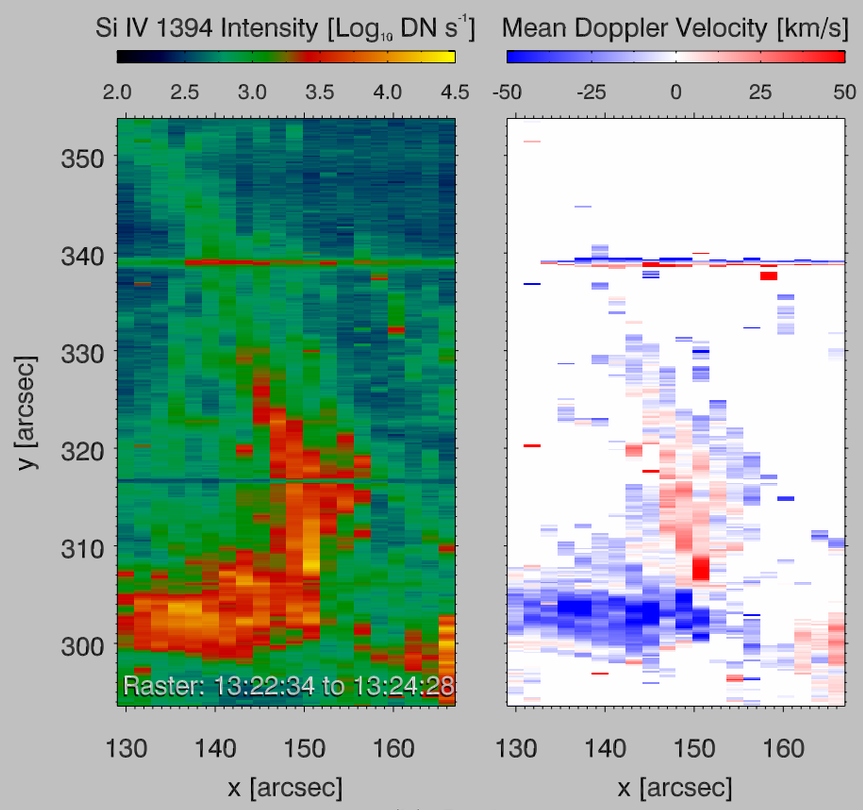

(b) Jet 2

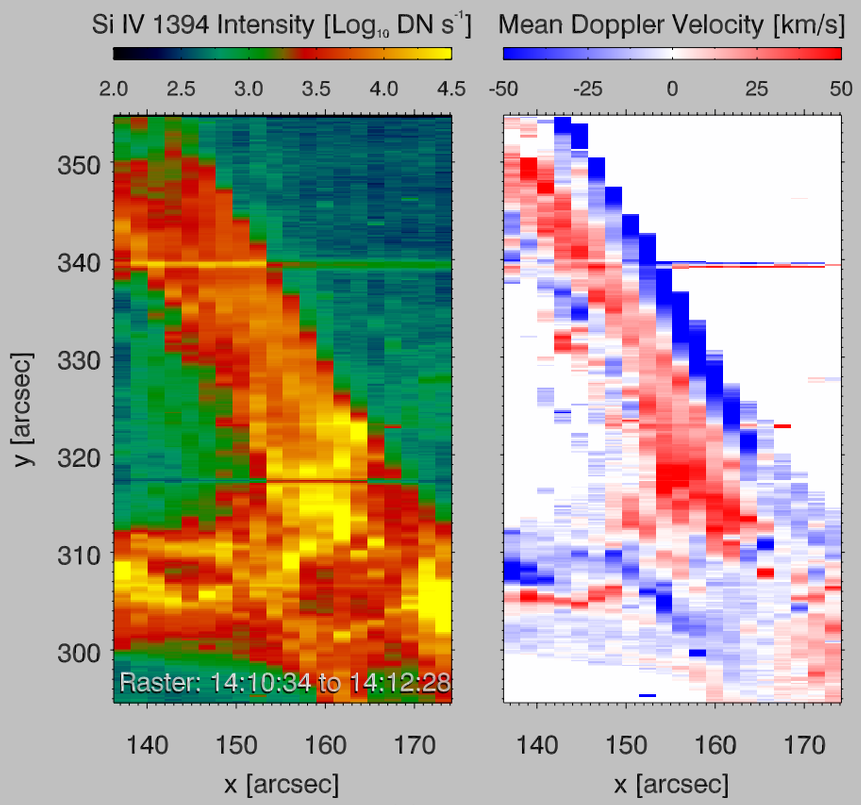

(c) Jet 3

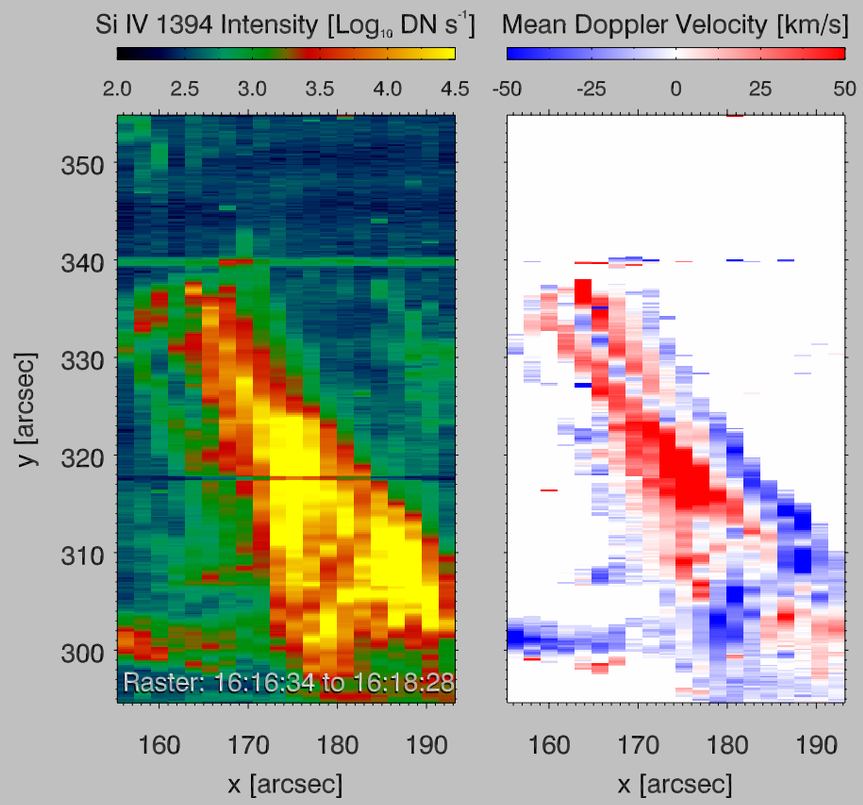

(d) Jet 4

Doppler shift maps using the Si IV 1394 line (log T ~ 4.9) observed by IRIS shows helical motion in all four jets (Cheung et al, in prep).

Hinode/SP vmag : 2013-07-21T13:18 to 2013-07-21T14:14

Red: $B_{los} < 0$

Blue: $B_{los} > 0$

Green: B_t

In a nutshell, the data and model support the mechanism proposed by Pariat et al. (2009, 2010) for homologous jets.

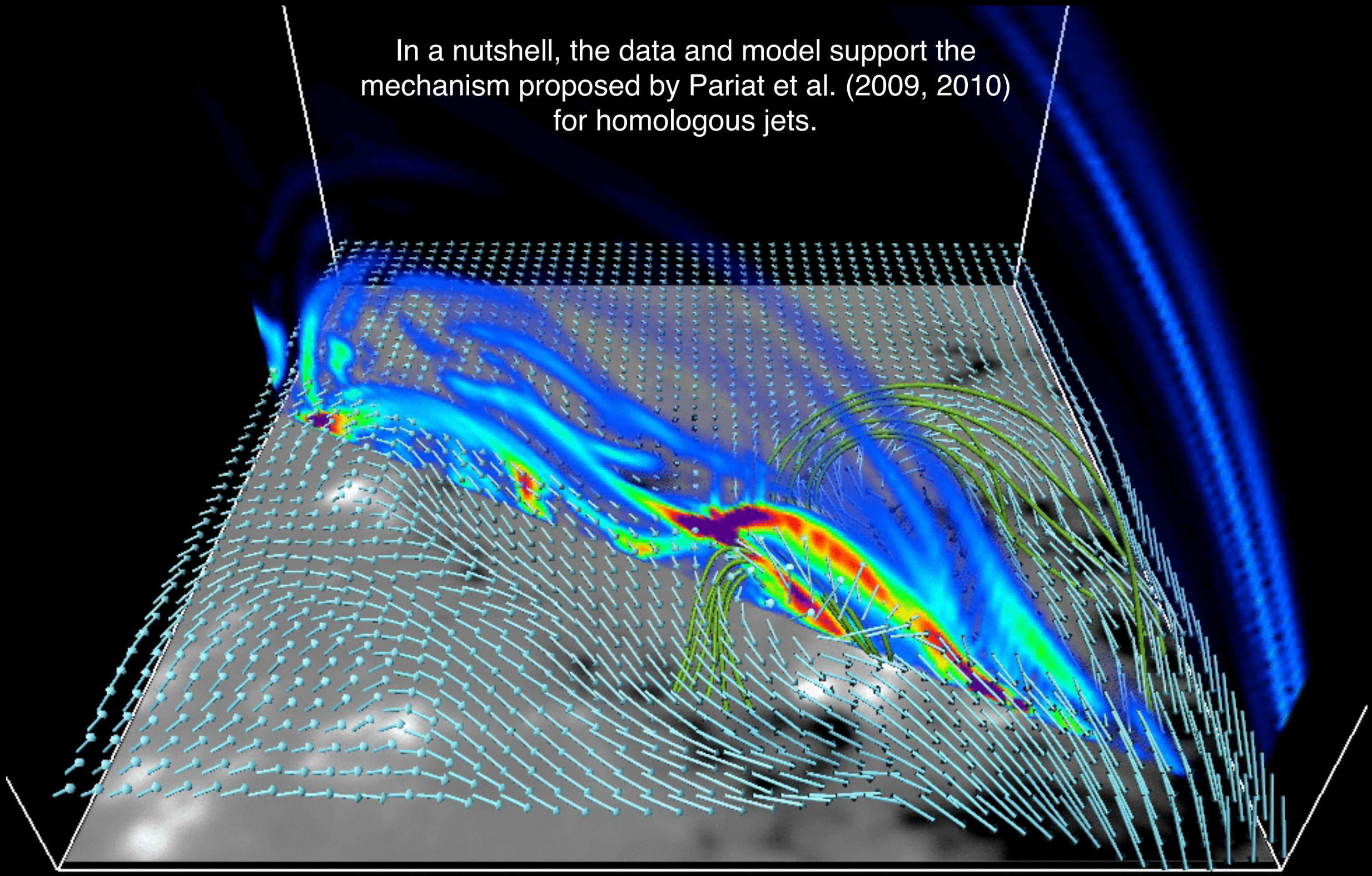

Magnetofriction model ($\nabla_h \cdot E_h = -U^* Jz$, U = 1.1 km/s) of homologous helical jets driven by HMI vector magnetograms (Cheung et al, 2015).

Data-Driven Simulations

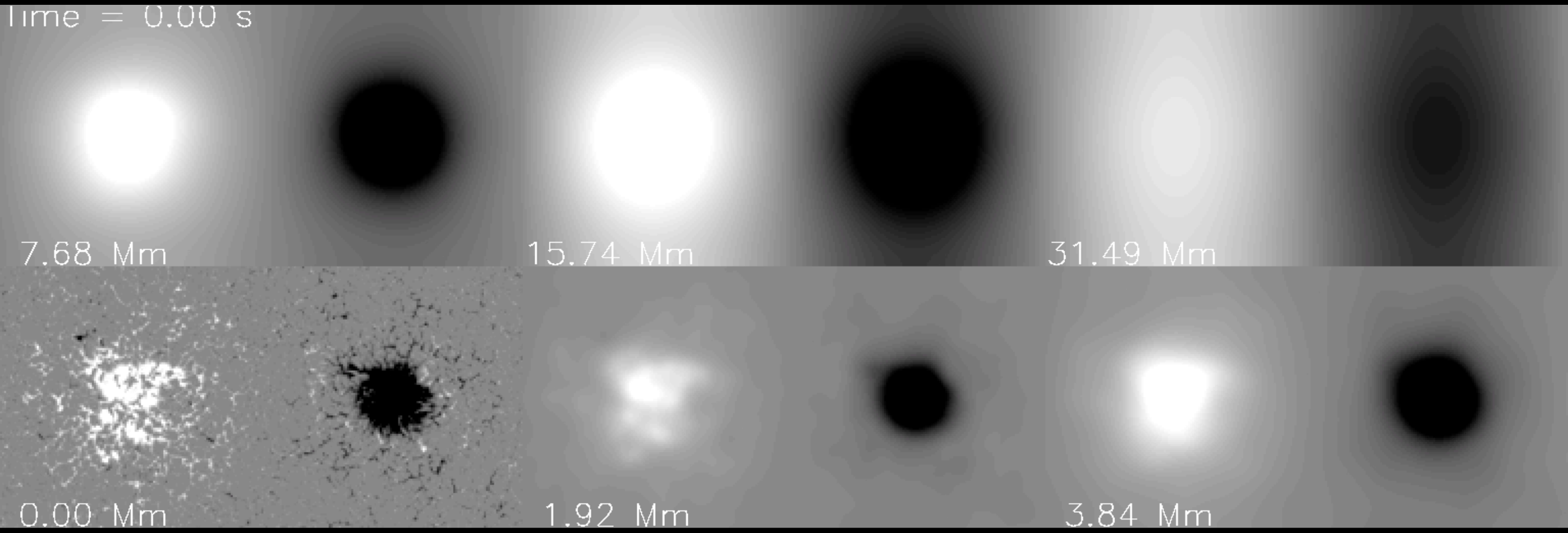

- Above: Using MHD quantities sampled at z=0 in a MURaM simulation, computed photospheric electric field to impose bottom boundary condition of a data-driven magnetofriction (MF) model (c.f. Cheung & DeRosa 2012, ApJ; Cheung et al. 2015, ApJ; Fisher et al. 2015 Space Weather).

- Data-driven fully-compressible MHD model under development (M. Rempel,. Chen, M. Cheung, FM. Kazachenko, G. Fisher).

High Performance Computing for Observational Solar Physics

ESA Solar Orbiter Implementation: Programmed space-qualified FPGAs to solve the polarized radiative transfer equations

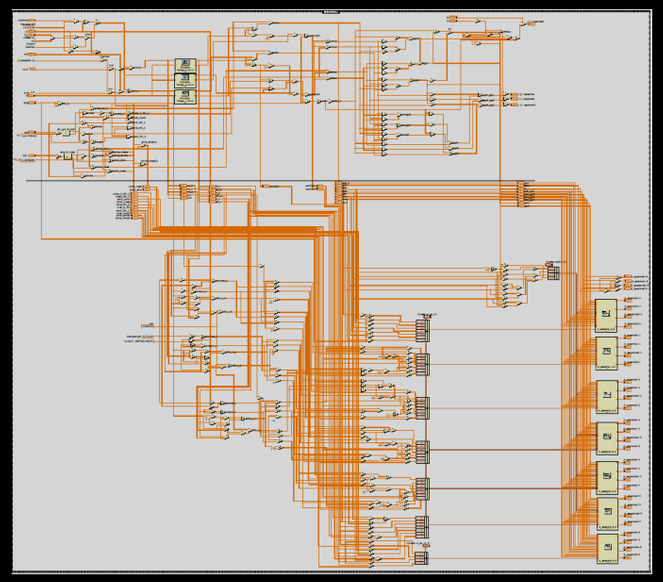

$$\frac{dI}{d\tau_c} = K(I - S)$$

Onboard inversion cuts telemetry requirements by factor of 6.

The Polarimetric & Helioseismic (PHI) instrument takes 2048x2048 pixel images: @ 4 Stokes parameters @ 6 wavelengths. Onboard inversion gives 4 physical quantities (vector magnetic field + doppler velocity). Data rate cut by 6 before lossless compression is applied The overall compression factor is 33 (JPB Carrascosa, 2015, doctoral thesis, U. Granada).

Stokes Polarimetric Inversion with DNNs

Problem: Can we use DNNs to do Stokes Polarimetric Inversions?

Differences from the Differential Emission Measure (DEM) problem:

- Forward problem is nonlinear
- #Outputs < #Inputs

Carroll & Staude (2001); Socas-Navarro (2005); Asensio Ramos (ongoing)

From radiative inversion

From DNN

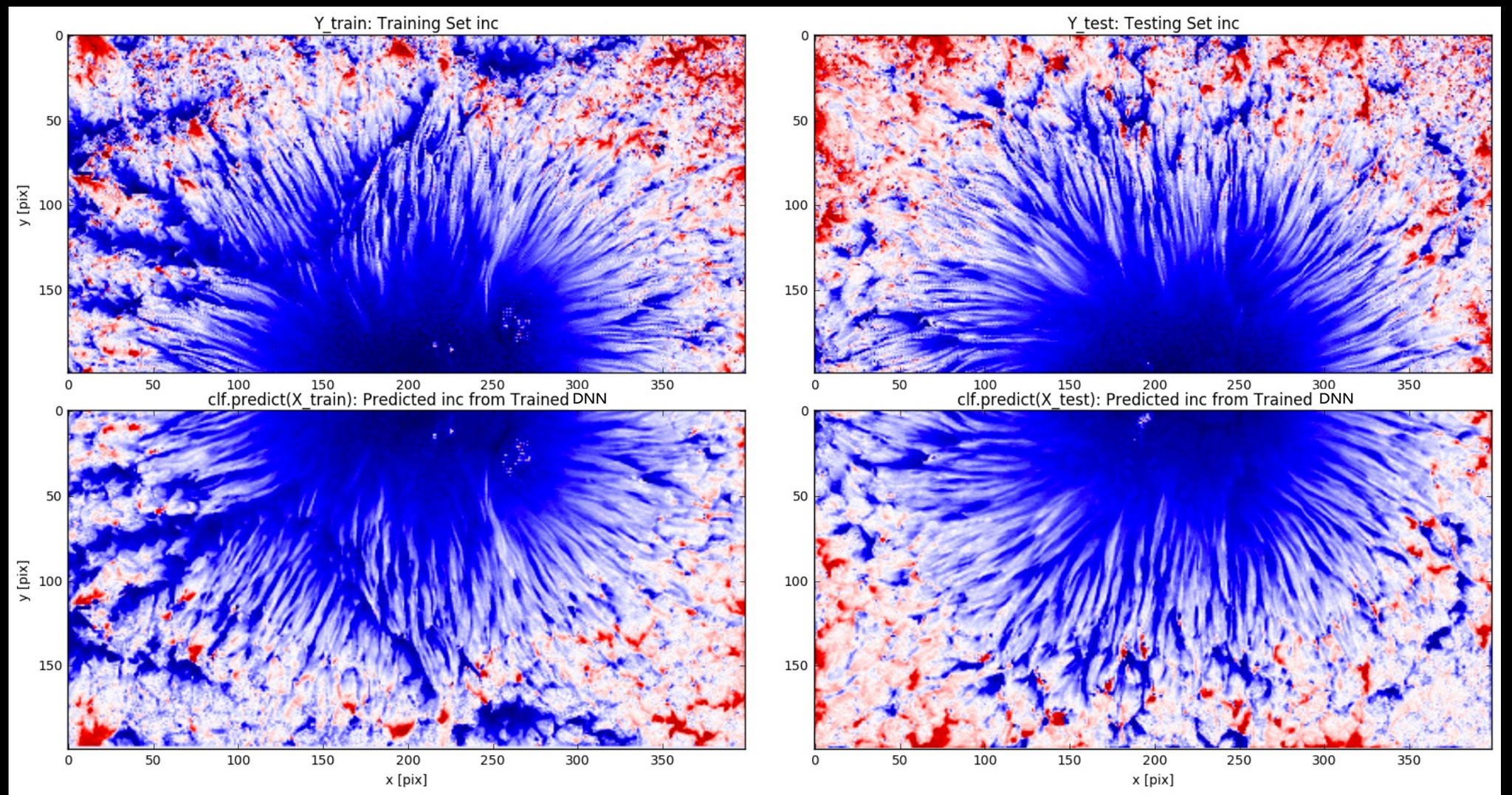

Training set

Testing set

Trained neural network for determining the inclination angle (red toward observer, blue is toward solar interior) of the magnetic field in (around) a sunspot.

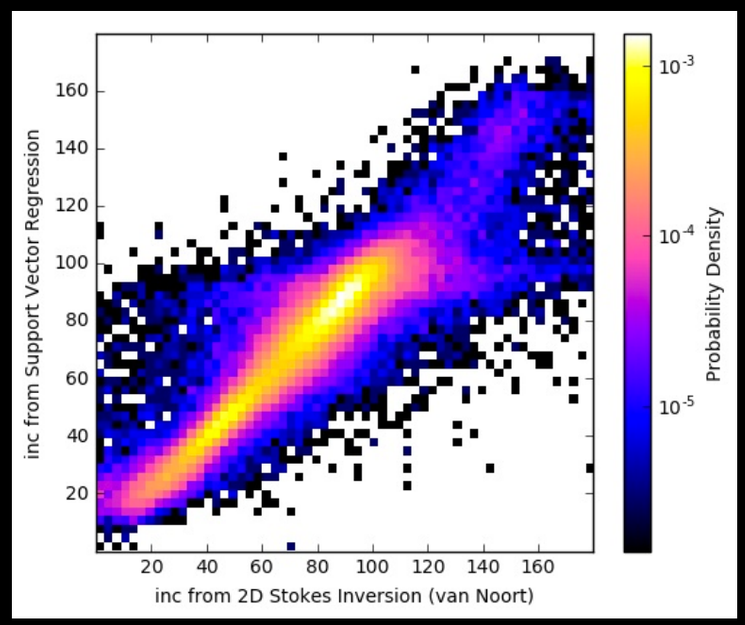

Some Concluding Remarks

- Many compelling science questions can be addressed given reliable maps of the chromospheric B field:
    - Even at a spatial sampling much lower than the EST / DKIST diffraction limit (e.g. IFU @ ~ 0.5 to 1 arcsec).
        - Take advantage of the 4m aperture as a light bucket to get high polarimetric sensitivity at high cadence (say, 30s).
- Consider using (photospheric magnetogram) data-driven models of EFRs to guide spectropolarimetric inversion / interpretation.

Some Concluding Remarks

- Example of a science topic that could be interesting for multiple communities? Magnetic Reconnection.
  - The chromosphere is our (solar + helio + astro-physicists) best shot for magnetic imaging of reconnection regions.
  - Better than the corona (lost some complexity already, low densities, optically thin), and
  - Better than the photosphere (B is not space-filling).
  - Much better than the magnetosphere (densities too low for imaging).
  - Much better than other astrophysical objects (time-scales, line-of-sight confusion).

Some Concluding Remarks

- Take advantage of advances in high-performance computing and machine learning techniques to:
  - Improve the throughput and efficiency of data processing pipelines (e.g. phase diversity or speckle reconstruction, Stokes inversion, Monte Carlo estimate of uncertainties),
  - Sift through huge data volume to identify regions of interest (c.f. http://www.lmsal.com/hek)
- Cultivate the solar physics community to have strong HPC and machine learning skills:
  - use industry-standard, open source frameworks,
  - attract good students and postdocs, let them move easily into other fields / industry if needed. Make boundary between solar physics and other STEM fields more porous.